Coronal Hole Properties in Solar Cycle 24:

Plasma Behavior in the Weakest Period of Solar Activity Over the Last Half Century

A Thesis Presented

By

Adrián Arteaga

To

The Department of Astronomy

in partial fulfillment of the requirements

for the degree of Bachelor of Arts

11 April 2014

Harvard University

ABSTRACT

Coronal holes, regions of low temperature and density in the solar corona which coincide with open and mostly unipolar magnetic field lines, are the primary source of the fast component of the solar wind. I have conducted a systematic study of the properties of coronal holes from 2007 to February 2014. As part of my study, I have created a catalog of 691 coronal holes, the largest in existence for the current solar cycle, cycle 24. For 363 of these coronal holes, I have characterized the proton density, speed, and temperature of the associated solar wind streams measured at 1 AU. For 189 wind streams, I have also been able to collect the ratio of alpha particle to proton number density in the wind. A comparison of these properties has shown that there is an anti-correlation between wind density and speed (higher densities correspond to lower wind speeds), and correlations between wind temperature and alpha to proton number density ratios and speed (higher wind speeds correspond to higher temperatures and larger alpha to proton number density ratios). In addition, a study of the relationship between area and magnetic field strength for the coronal holes of these past seven years has revealed that smaller coronal hole areas correspond to larger magnetic field strengths. I have also found that coronal holes with higher magnetic field strengths produce lower wind speeds, while coronal holes with larger areas generate higher wind stream velocities.

CONTENTS

1 INTRODUCTION

Coronal holes are regions of low density plasma in the solar corona with open magnetic field where the high-speed component (550 - 800 km/s) of the solar wind is accelerated before escaping into interplanetary space. In on-disk X-ray and ultraviolet images of the corona, they appear as discrete dark patches on the solar disk. In off-limb coronagraphic observations they appear as low-intensity, low-density cone-like regions spatially connected to the dark patches seen in on-disk observations. Due to its low density, coronal hole plasma is nearly collisionless, and consequently, each ion species in the gas retains its own specific set of values for properties such as temperature and outflow speed. The values and ratios of abundance of these ion species provide a signature by which to identify coronal hole plasmas.

Coronal holes are indistinguishable from surrounding regions in on-disk images at temperatures below $10^5\ K$, but in visible light coronagraphic studies, large coronal holes appear as conical regions of negligible intensity extending beyond the solar limb (see figure 1.1). They were first identified in this form in 1956 by M. Waldmeier at the Swiss Federal Observatory in Zurich (Cranmer 2009). Early visible light studies of the corona provided little insight into the nature of coronal holes, but as early as 1958 a connection was drawn between coronal holes and radially expanding magnetic field lines following the observation of solar plumes tracing these lines in the largest of coronal holes (Saito 1958).

The first observations of on-disk coronal holes occurred in the late 1960s, with the advent of rocket borne ultraviolet and x-ray detectors. These early observations determined that electron densities and temperatures were lower in coronal holes than in

the rest of the corona (Munro & Withbroe 1972), confirmed that the coronal holes coincided with regions of open magnetic flux (Wilcox 1968; Altschuler *et al* 1972**;** Hundhausen 1972), and established a causal link between high-speed solar wind streams and the largest coronal holes (Noci 1973**;** Pneuman 1973**;** Krieger *et al* 1973). The first extended in-depth study of coronal holes was carried out using the Apollo Telescope Mount aboard the Skylab space station between 1973 and 1974 (Huber *et al* 1974). This study solidified theories about coronal holes from the previous decade with a large volume of high-quality data (Cranmer 2009).

Following a lull in the research after the late 70s, the study of coronal holes was revitalized in the 90s with the launch of a flotilla of over a dozen heliophysical satellites.

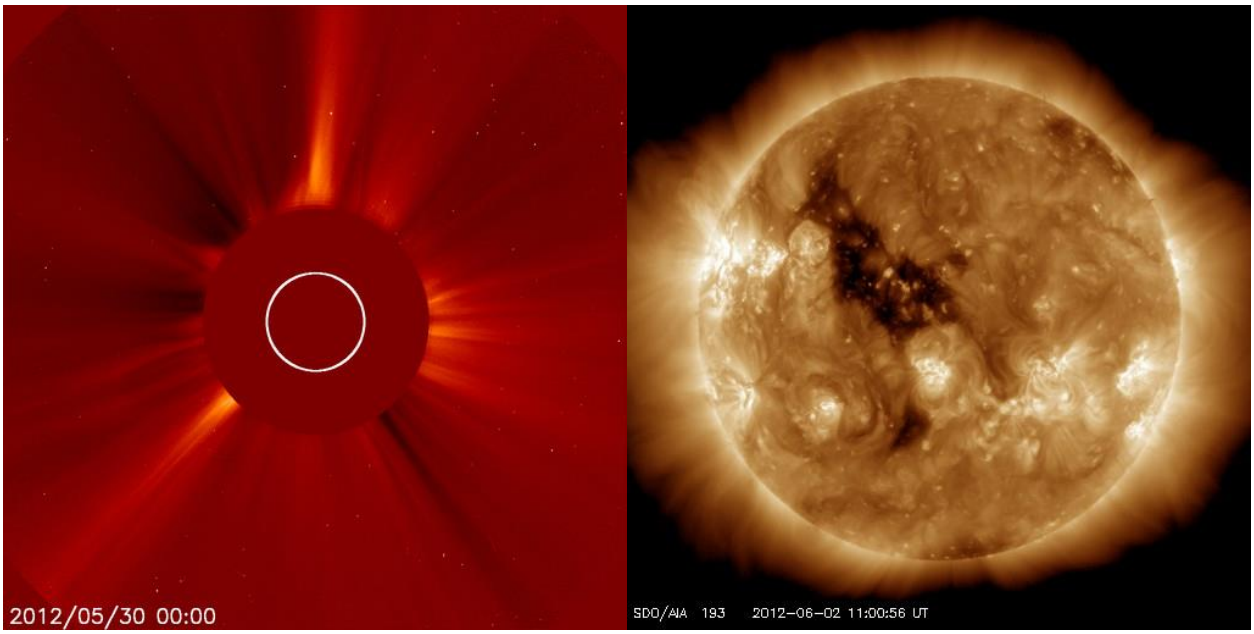

Figure 1.1 Left: Visible light coronagraphic study taken by the LASCO C2 instrument aboard SOHO, which images the solar corona from 2.5 to 6 solar radii. The white circle at the center of the picture indicates the spatial extent of the solar disk. The dark streams in the upper-left and lower-right of the image are coronal holes as observed off the solar limb. Right: On-disk observation of the solar corona taken by the SDO/AIA instrument at a wavelength of 193 Å (~1.5 million K), the large dark patch on the solar disk is a coronal hole. This picture, taken three days after the one to the left, shows a head-on view of the same coronal hole that is seen transversely in the upper-left of the previous image.

The Ulysses (1990, past), SOHO (1995, operating), and ACE (1997, operating) missions were particularly instrumental in the development of the field and allowed for detailed and continuous monitoring of the solar corona over several years. Extended observations of the corona in the first decade after the launch of these satellites established that coronal holes vary in their location on the Sun and in their morphological and plasma properties over the length of the solar cycle (Miralles *et al* 2001a, b, 2002, 2004, and 2010).

The solar cycle is the variation in levels of solar activity over a period of approximately 11 years. It is driven by the change in polarity of the solar magnetic field (see figure 1.3). During solar minimum, when the solar magnetic field is characterized by a strong dipolar component and photospheric activity is at its lowest, the largest coronal holes are found only at the poles of the Sun. At this time, there are few to no coronal holes in the lower latitudes, and these are generally small and short-lived. Over the next five years, as the magnetic field weakens at the poles and the solar magnetic dipole is replaced by more complex and chaotic magnetic configurations, coronal holes migrate to the lower latitudes. For approximately 3 to 4 years around solar maximum, the poles are bereft of coronal holes, which during this time are predominantly found near the equator, and more rarely at higher latitudes. Within less than a year after solar maximum, following polarity reversal of the solar magnetic field, high-latitude coronal holes become more common. Many of these high-latitudes holes gather and migrate to the poles, forming large polar coronal holes that grow until solar minimum, and which last until the advent of the next cycle's maximum. The growth phase of polar coronal holes has been found to

last approximately twice as long as their decline phase after solar minimum (Fisher & Sime 1984**;** Miralles *et al* 2001a).

The first description of the reappearance of a polar coronal hole from the migration of a high-latitude coronal hole (see figure 1.2) which incorporated spectroscopic measurements of ion outflow velocities and temperatures was given by Miralles *et al* (2001a). These authors were also the first to describe the significant outflow velocity differences between low-latitude, and polar coronal holes (Miralles *et al* 2001a, b).

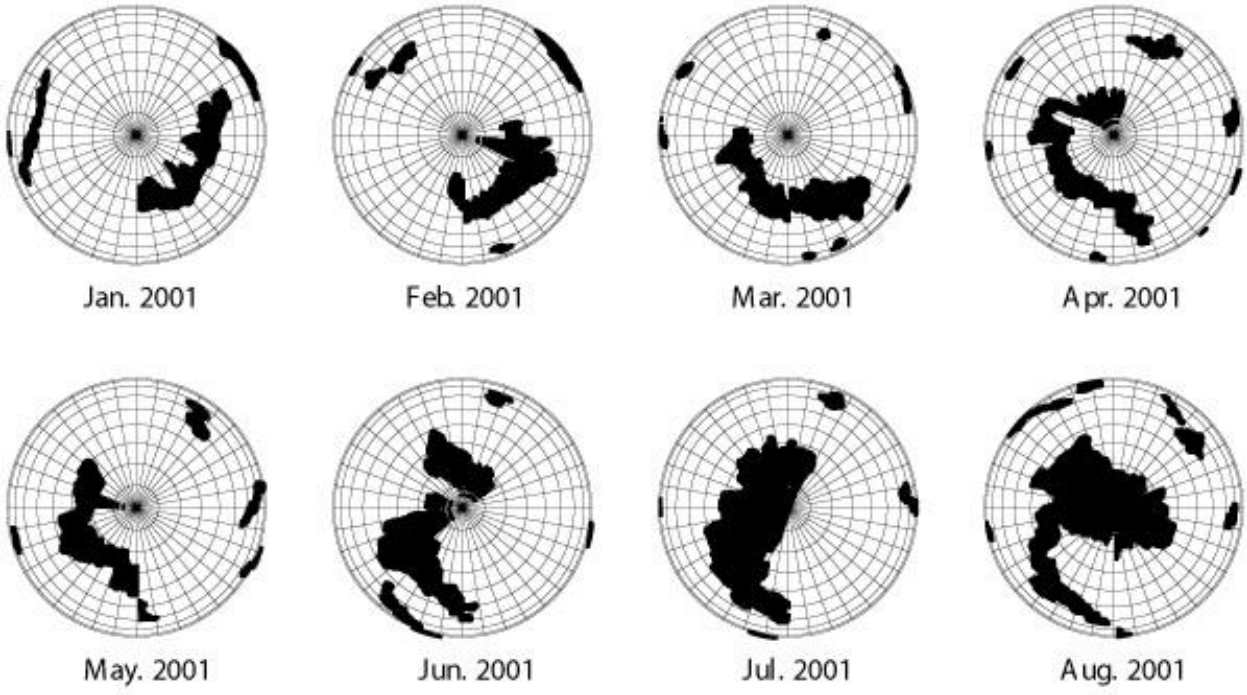

Figure 1.2 View of the formation of a large polar coronal hole from smaller high latitude holes using reconstructed coronal hole boundaries from Kitt Peak He 10830 Å maps. From Cranmer 2009.

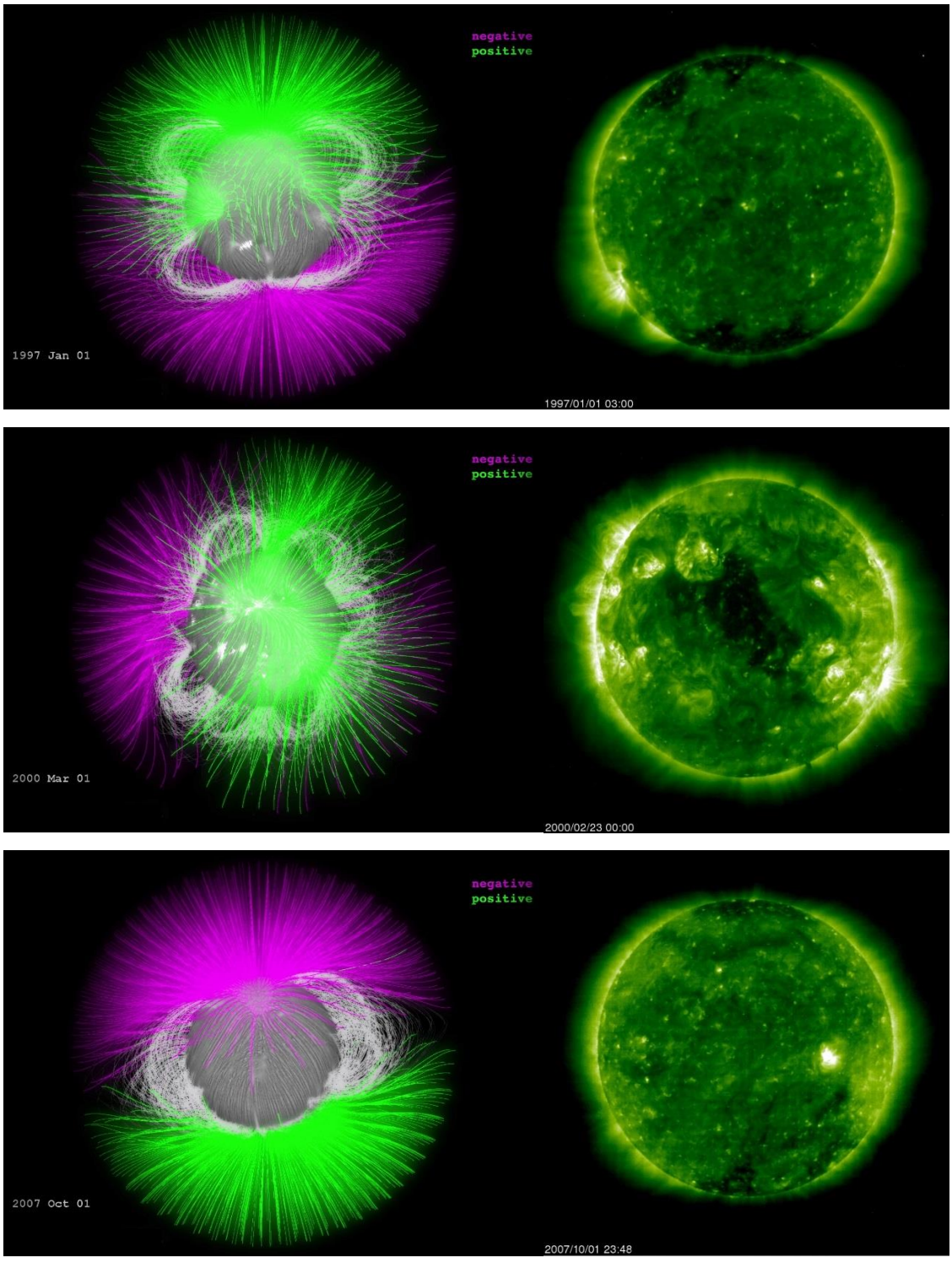

Figure 1.3 (*Left), top to bottom*. The evolution of the solar magnetic field over a period of 11 years, which defines the solar cycle. The top and bottom frames show the field configuration during solar minimum, the central frame during solar maximum of solar cycle 23. (*Right), top to bottom.* Spatial distribution of coronal holes over the solar cycle. The top and bottom frames correspond to solar minimum, when large coronal holes tend to dominate the poles. The central frame corresponds to solar maximum, when large coronal holes can be found in the lower latitudes. *Magnetic field maps courtesy of the NASA's Goddard Space Flight Center Scientific Visualization. Coronal hole images taken by SOHO/EIT.*

Using spectroscopic diagnostics from data taken by the Ultraviolet Coronagraph Spectrometer (UVCS) aboard *SOHO* of O+5 outflow velocities for polar and low-latitude coronal holes in solar cycle 23, Miralles et al. (2001a, 2004) were able to determine that from 1.5 to 3 solar radii polar coronal holes exhibit the fastest outflow speeds and equatorial holes the slowest, with mid- and high-latitude holes bridging the gap between the two (see figure 1.4). From in-situ observations of solar wind velocities, it was known that both large polar and equatorial holes produced winds with velocities of ~700 km/s at 1 AU, yet at 3 solar radii, the wind from polar coronal holes reached velocities of ~400 km/s, while the wind from equatorial holes remained at approximately ~100 km/s. This finding established that solar wind acceleration occurs for the most part beyond 3 solar radii in low-latitude coronal holes, but is split evenly for polar holes. In addition, from the cataloguing of ~200 large low-latitude coronal holes from 1997 to 2007, these authors (Miralles et al. 2006, 2007) were able to determine several other important trends about the properties of coronal holes: 1) coronal holes with lower densities at a given heliocentric distance tend to exhibit faster ion outflows and higher ion temperatures (see figure 1.5); 2) the heavy ions in coronal hole plasmas show a strong correlation between their heating and their wind speed; and 3) low-latitude coronal holes do not seem to reach the extreme plasma parameters observed for polar coronal holes (see figure 1.4). These studies for cycle 23 also showed that large and long lived low-latitude coronal holes were only found in large numbers in the rising phase of the cycle, during solar maximum, and the declining phase of the cycle. However this trend was broken in solar cycle 24, where many large low-latitude coronal holes were observed during the minimum phase.

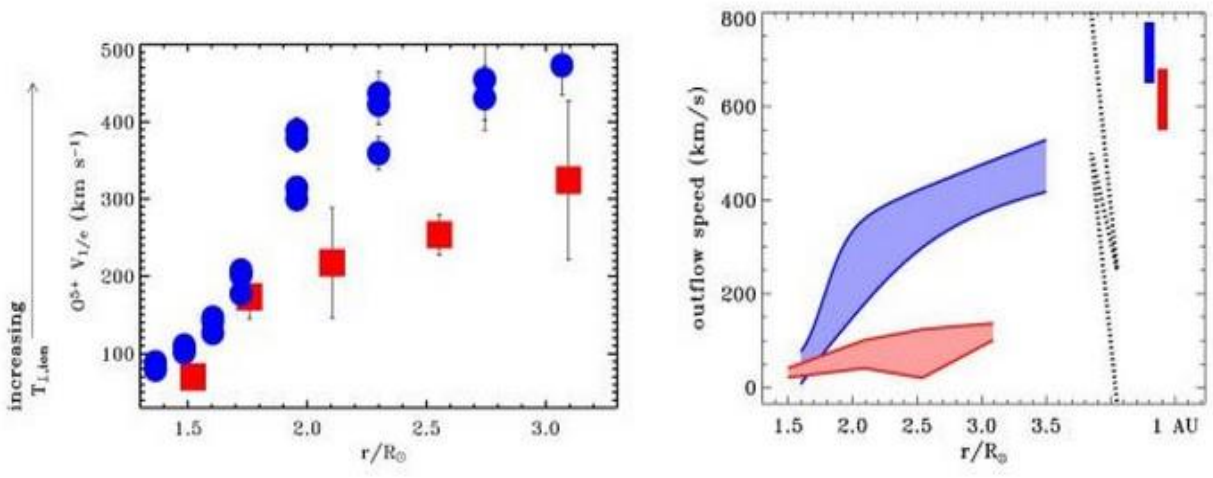

Figure 1.4 V1/e linewidth velocity (left) and O+5 outflow velocity (right) derived from O+5 intensities and widths using UVCS/SOHO for polar coronal holes during solar minimum (blue) and equatorial coronal holes during solar maximum (red). Ranges of 1 AU solar wind speeds (from Ulysses and ACE) are show to the top-right of the right panel. From Miralles et al (2006).

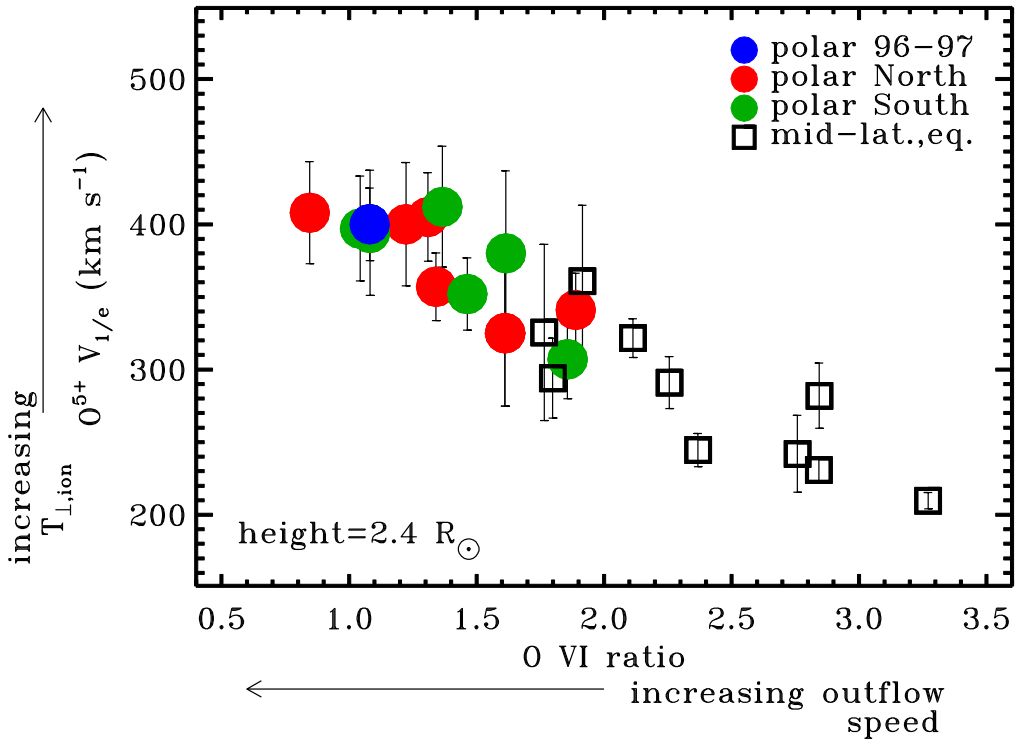

Figure 1.5 O+5 1032 Å line widths versus line ratio at 2.4 solar radii for coronal holes at different stages of solar cycle 23. Polar coronal holes: solar minimum (blue circles), new polarity north (red circles), new polarity south (green circles); Low-latitude coronal holes: mid-latitude and equatorial (squares). From Miralles et al (2006).

Without more data from other cycles, it is difficult to determine whether the presence of large equatorial holes during the recent solar minimum is truly anomalous, or whether it occurs regularly over a period of cycles. Interestingly, cycle 24 has so far displayed other anomalous behavior. The cycle is on track to have the lowest sunspot count since cycle 14, more than a hundred years ago, and the magnitude of the net magnetic field at the poles for the current cycle is approximately 50% weaker than that of the previous cycle (see figure 1.6). Additionally, solar wind mass flux is 20% lower for the current minimum when compared to the previous one (McComas *et al* 2008).

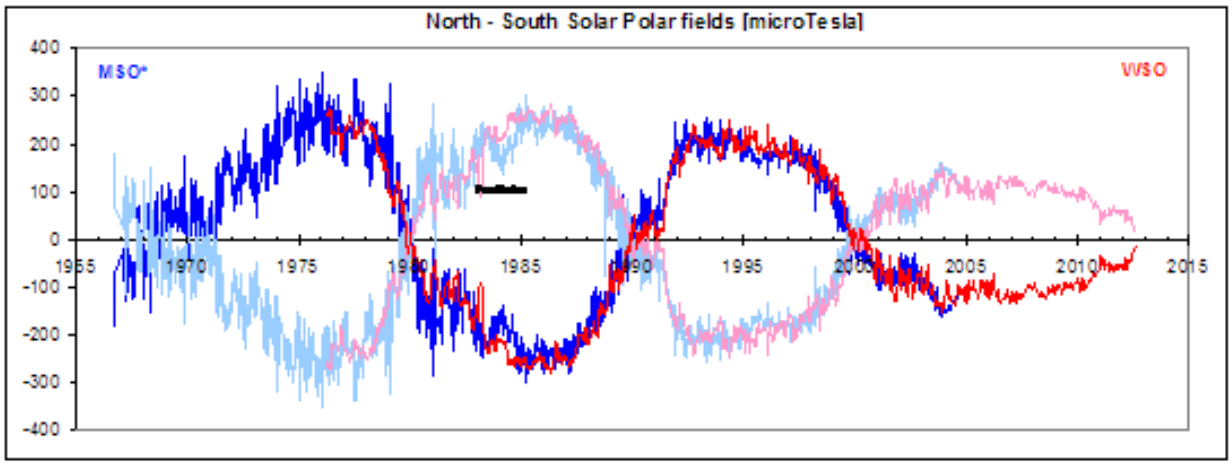

Figure 1.6 Polar magnetic field magnitude over the last 60 years, using measurements from the Mount Wilson Observatory and the Wilcox Solar Observatory. Notice that aside from being fifty percent weaker than the field of the previous cycle, the current cycle's magnetic field is also the weakest since magnetic field observations began at Mt. Wilson in the 1970s.

For my thesis, I have carried out a complete investigation of all low-latitude coronal holes from January 2007 to January 2014. The presence of large low-latitude coronal holes in the minimum of the current cycle provided a rare opportunity to study how changes in the magnitude of the solar magnetic field affect the properties of coronal holes.

Coronal hole plasma properties such as ion temperatures and abundance ratios, or outflow velocities, have long been used as constraints for models seeking to describe the physical processes which dictate the behavior of the solar corona. Due to the abnormal conditions of current solar cycle a study of the plasma behavior of the coronal holes in this cycle would provide a new and unique set of more robust constraints. Current solutions to the coronal heating problem, the 70-year-old puzzle of how the corona is heated to million degree temperatures when the solar photosphere burns at a relatively cool 6,000 K**,** attribute coronal heating to either magnetic reconnection processes or Alfvén waves from deep within the photosphere. Since both processes have so far been able to replicate some aspects of the coronal plasma properties it is difficult to determine which one of the two could be the principal mechanism. The introduction of new constraints to these models may help in discriminating between the two by showing that one is able to more effectively replicate the properties of coronal hole plasma under the peculiar phenomenology of the current cycle.

In my survey of coronal hole properties, I dedicated special attention to small, transient coronal holes. These holes are a source of low-speed, high-density solar wind, and at first glance their properties seem to appear to bridge the gap between coronal streamers, and the more traditional fast wind, low density coronal holes. Traditionally, their study has been neglected due to the difficulty of correctly sampling their plasma separate from foreground and background structures. For in-situ observations of solar wind coming from small coronal holes, for example, the fast flows from nearby larger holes often overtake the slower wind of the smaller holes, making it difficult and time consuming to obtain clean sections of uninterrupted data for the wind emanating from the

smaller holes. By searching for them over a seven year period, I was able to study many of these smaller holes, even though only clean data was available for a fraction of their total number. Finally, I was able to establish many important trends relating the properties of coronal hole wind streams as they are detected at 1 AU (wind speed, density, temperature, and elemental ratios), and the physical properties of the coronal holes in the solar atmosphere (area and magnetic field strength).

2 METHODOLOGY

This section offers a description of the strategies and techniques I used to collect and analyze data. The data used in my research falls roughly into three main categories: extreme ultraviolet (EUV) images of the solar corona, 1AU measurements of solar wind properties, and magnetic maps of the solar photosphere. The sections in this chapter reflect these three major divisions.

2.1 EUV DATA COLLECTION

The first goal of this project was to create a catalog of all coronal holes from the year 2007 to the present. This was achieved by manually scanning for coronal holes through thousands of extreme ultraviolet images of the solar corona captured by the SOHO and SDO missions over the last seven years.

For the time span between January 2007 and June 2010, I used 195 *Å* images taken by the Extreme Ultraviolet Imaging Telescope (EIT) aboard SOHO. This instrument has a frame rate of 1 picture every 12 minutes, and a resolution of 2.6 arcseconds per pixel (1024x1024 pixel image size). From June 2010 to February 2014, I used 193 *Å* images from the Atmospheric Imaging Assembly (AIA) instrument aboard SDO, which has a frame rate of 1 frame every 12 seconds and a resolution of .67 arcseconds per pixel (4096x4096 pixel image size).

The identification of coronal holes was a time consuming process. For any particular year, I would download a week of EIT or AIA data, and scan through each frame looking for coronal holes. As shown in figure 2.1, coronal holes appear as very obvious

dark patches on the otherwise (false color) bright green (EIT 195 *Å*) or bronze (AIA 193 *Å*) solar surface.

After identifying a coronal hole in these EUV images, I selected the frames corresponding to the dates of when the hole's leading edge first reaches the solar meridian, and when its trailing edge last crosses over it (see figure 2.2). The dates stamped in these frames, henceforth referred to as D1 and D2, were converted into fractional day of year dates and stored. This process was repeated for every week of every year from 2007 to 2014. The result was a database consisting of a coronal hole identification number, and a start and end date associated the hole's crossing of the meridian.

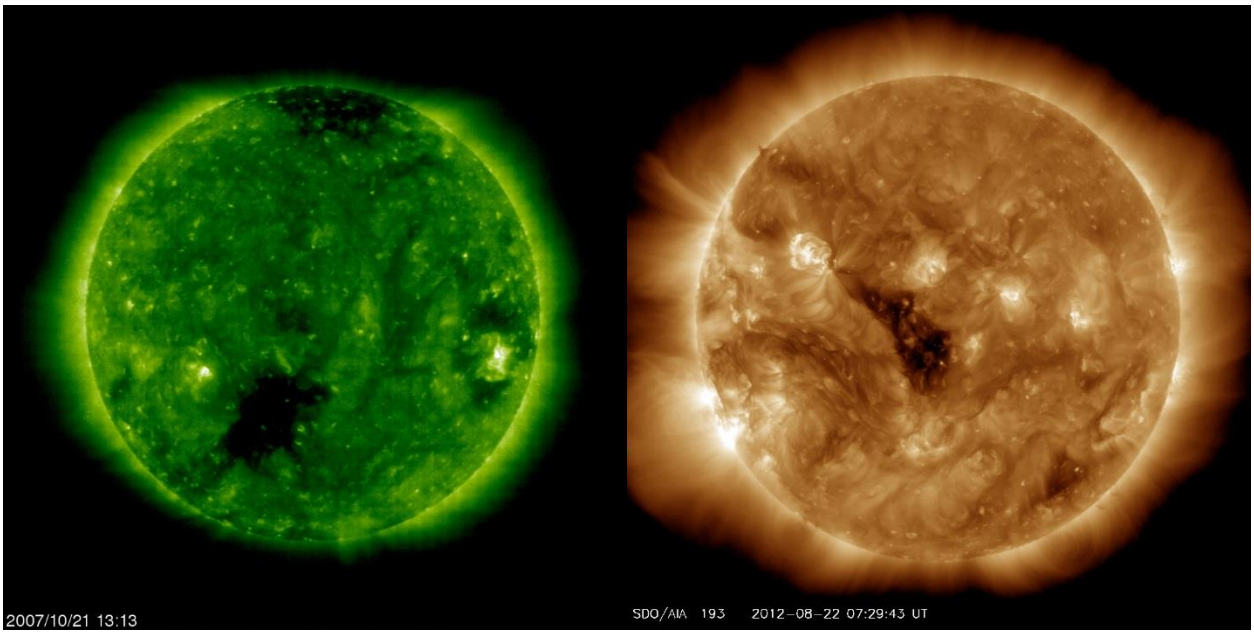

Figure 2.1 Sample of SOHO/EIT 195 *Å* (left) and SDO/AIA 193 *Å* (right) images used to search for coronal holes.

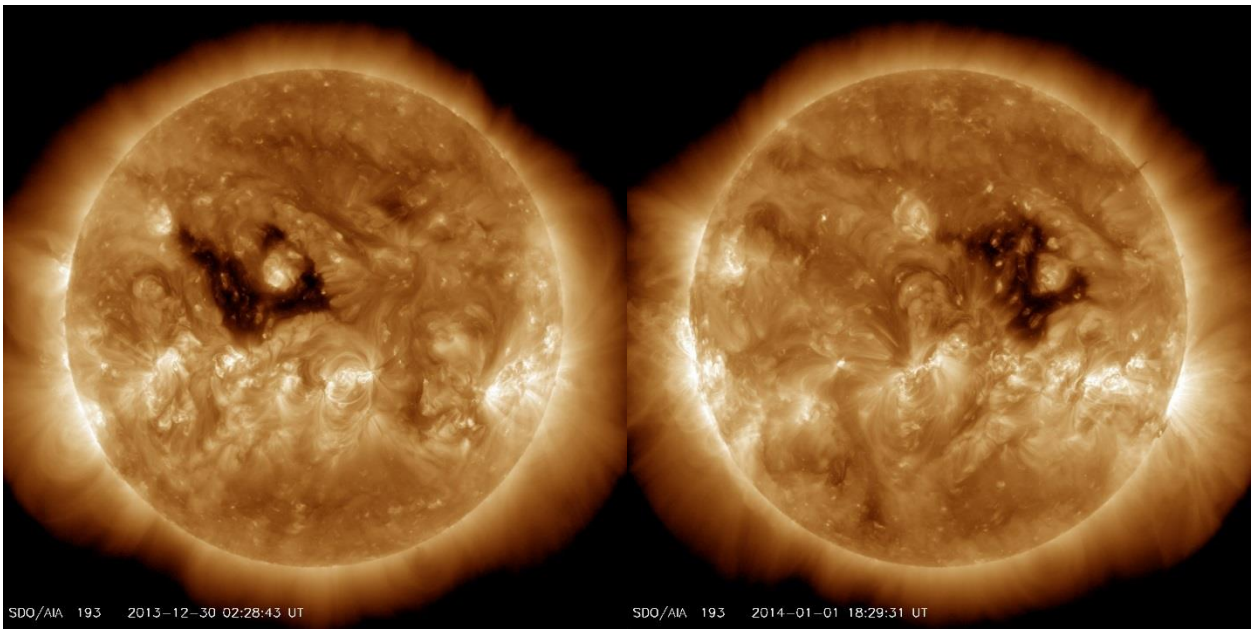

Figure 2.2 SDO/AIA frames capturing the moments when the leading edge of a coronal hole first reaches the solar meridian (*left*) and when trailing edge last crosses it (*right*). The dates stamped in the lower left of each image, are the respective D1 and D2 recorded for this particular hole (the 108th coronal hole for the year 2013).

Since coronal holes can persist over many months, several meridian crossing events per year correspond to different sightings of the same particularly long lived holes. In this study, I am mainly interested in the relationship between coronal hole area, magnetic flux, and hole wind-stream properties. Coronal holes are very dynamic structures, an initially large polar coronal hole many diminish in size and move to lower latitudes over time, displaying different properties each time it is spotted every solar rotation. To control for this constant change in hole properties, I have chosen to consider each sighting of a coronal hole meridian crossing event as a unique coronal hole.

Figure 2.3 shows the yearly breakdown of coronal holes in my EUV catalog. For the seven years and one month I surveyed, I was able to identify a total of 691 holes. Currently, this is the largest survey of the coronal holes of solar cycle 24.

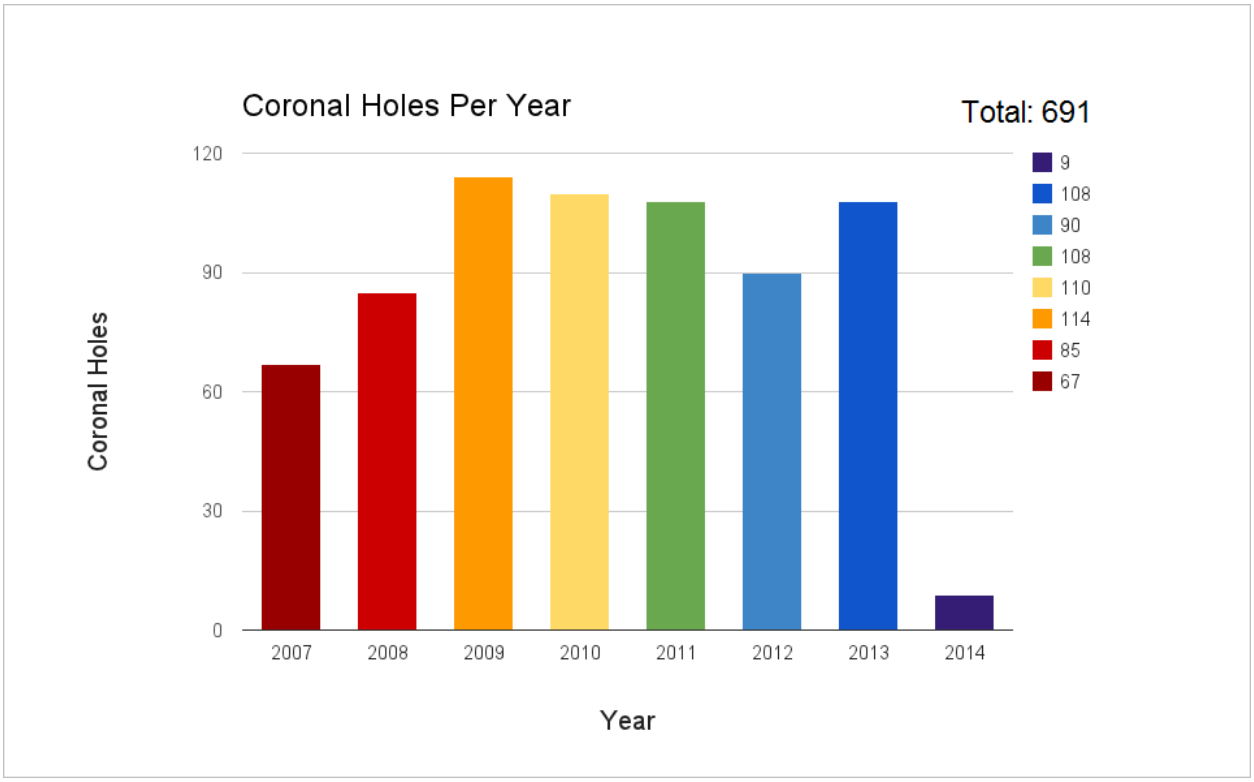

Figure 2.3 Number of coronal hole events cataloged for each year in my survey. Only the month of January is included for the year 2014.

The number of coronal holes per year varied significantly over the time span surveyed. The years 2007 and 2008 exhibited fewer holes than any other years, but the holes found during these years were larger and longer lived than those of other years. In contrast, the coronal holes from 2009 and the first half of 2010 were on average smaller, more irregular, and shorter lived than the holes of any other years in the survey. The years 2011, 2012, and 2013 bridged the gap between these two extremes, showing both large and small holes. The holes I sampled for January 2014 seem to resemble those found in 2007 and 2008; they were few and large.

2.2 CORONAL HOLE WIND DATA COLLECTION

The next step of the project consisted of studying the properties of the solar wind emanating from the cataloged coronal holes. Two instruments on two different spacecraft were used for the collection of solar wind data: the *Mass Time-Of-Flight Proton Monitor* (CELIAS MTOF/PM) aboard SOHO, and the *Solar Wind Electron, Proton and Alpha Monitor* (SWEPAM), aboard ACE. The CELIAS MTOF/Proton Monitor collects solar wind proton density, thermal velocity, and bulk speed with 30-second temporal resolution. The Proton Monitor data I worked with was further averaged first to 5 minutes, and then to 1-hour averages. The SWEPAM instrument collects the same properties as the CELIAS PM, but with the addition of ratios of alpha particle to proton number density. ACE/SWEPAM has a temporal resolution of 64 seconds, but the data I used consisted of 12 minute averages. Both satellites orbit the L1 point between the Earth and the Sun collecting solar wind data continuously.

To make the association between a wind-stream detected by the spacecraft at L1, and a particular coronal hole from my EUV catalog, I plotted the wind velocity and density values recorded by the instruments for a three week period centered around the dates D1 and D2. I then used an algorithm which based on D1and D2, and a user suggested velocity, would predict the arrival window of the wind at L1. The red shaded areas in the lower two panels of figure 2.4 indicate the wind arrival ranges predicted by the algorithm for the wind stream associated with the coronal hole sample shown in the top panel. The deeper red corresponds to a wind velocity of 600 km/s, while the lighter red corresponds to wind with velocity of 400 km/s. For most coronal holes, this range was sufficient to accurately predict their wind stream arrival window. Very large holes have faster wind

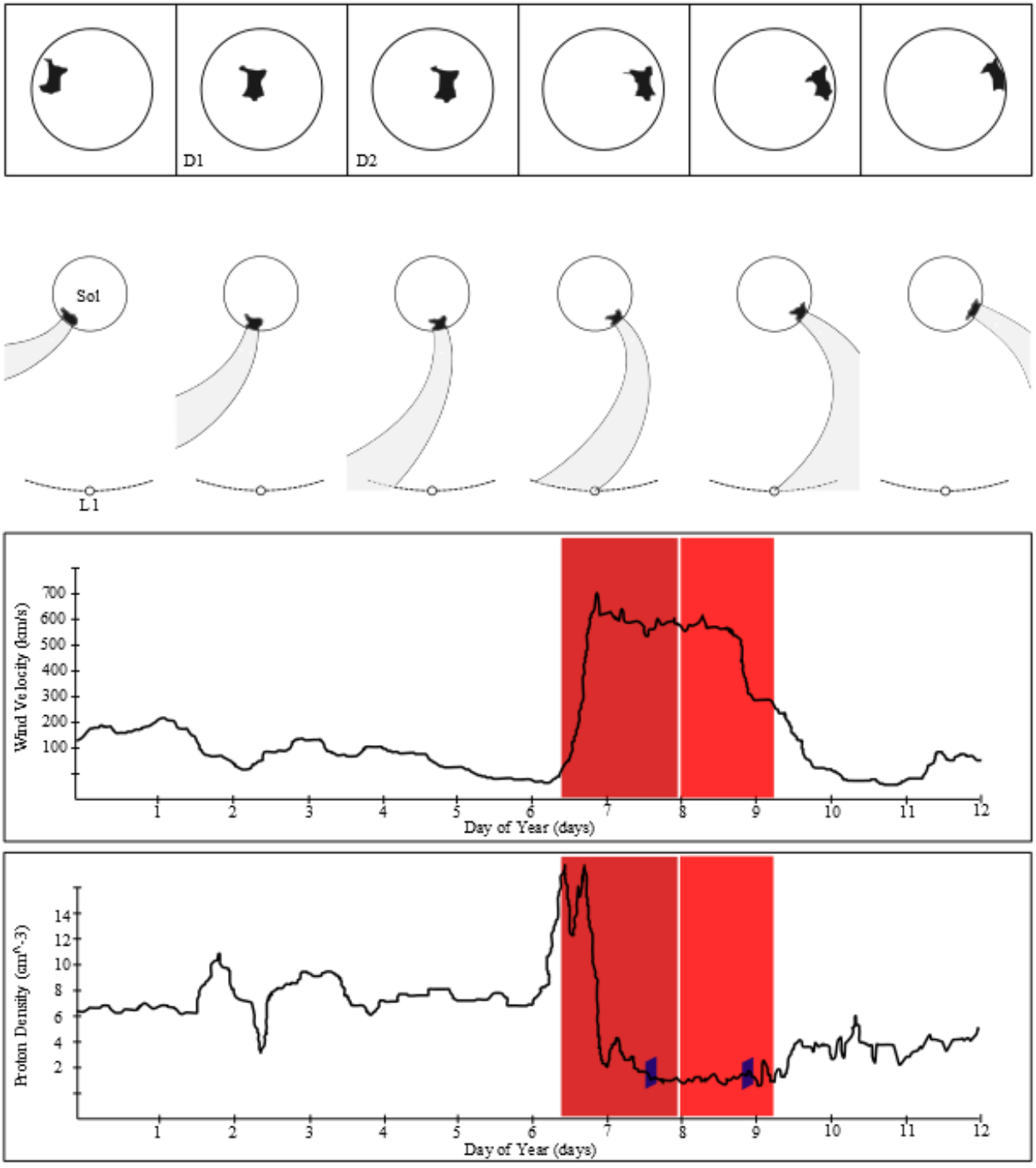

Figure 2.4 A stylization of the detection of a coronal hole in EUV images and the arrival of its wind at 1 AU. The topmost panel shows what the coronal hole looks like in EUV images of the solar corona as it transits over half a solar rotation. The frames stamped with D1 and D2 are the ones which would have been stored in my coronal hole image catalog. The second panel shows a bird's eye view of the solar system, highlighting the trajectory of the coronal hole's wind stream as it sweeps by the satellites as a function of time. The last two panels show the wind velocity and densities recorded by the satellites at 1AU. The red bars in these panels show the predicted arrival windows for the stream shown. The blue brackets enclose the actual time range selected for data analysis

(~700 km/s), and very small holes slower wind (~300 km/s), so the velocity range for such outliers was altered in order to reflect their slightly early, or late, arrival times.

The prediction algorithm was a powerful tool for quick visual identification of coronal hole wind streams, but the selection of the actual time range to sample for wind properties was done manually by me. The blue brackets in the bottom panel of figure 2.4 correspond to the actual time range I selected for the particular sample stream shown. I selected this region because it avoids the initial density shock from when the wind stream's leading edge first reaches the satellite. This shock front that precedes all coronal hole wind streams is caused by the compressive interaction between the fast wind from the stream, and the pervading interplanetary slow solar wind component, through which the fast wind pushes through. It must be avoided because it contains densities, temperatures, and velocities which are not representative of the stream's actual density, temperature, and velocity (they are much higher). The region enclosed by the blue brackets corresponds to a period of steady high velocity flow and relatively low wind densities which follows the wind shock front and last until the stream has moved on. The relative ratios between the velocity, density, and temperature from this region are unique to each different coronal hole, but the variation is not random, and can be characterized. Unfortunately, many holes do not exhibit an extended period of steady state plasma flow from which to draw wind stream properties. The length of this period is directly proportional to the size of the hole, so the useful collecting area was smaller for the smaller holes in my catalog. Additionally, in certain cases, due to interaction with wind streams from nearby holes, or with sources of high density slow wind, a wind stream's plasma was so thoroughly shocked that it was impossible to collect data. Since wind

expands super radially from its source region on the corona, the wind from certain high latitude holes sometimes missed the spacecraft, resulting in no detection at all. Finally, there were various data gaps all throughout the survey, so for certain streams there was simply no recorded data.

Despite these obstacles to data collection, I was still able to characterize the wind properties for 363 of the 691 holes cataloged on the extreme ultraviolet. Figure 2.5 shows the annual distribution for these wind streams. Onward from the year 2010, the quality of ACE/SWEPAM data deteriorated significantly, with many data gaps preventing me from characterizing many wind streams. Due to this deterioration, I decided not to look at ACE data for the year 2013. There are no available data from ACE for 2014.

Unlike when first looking for coronal holes in the EUV, where I used two different satellites to identify coronal holes from different time spans, I used ACE/SWEPAM and SOHO/CELIAS PM to look at the exact same wind streams. Thus for many of the streams I have two sets of velocities, densities, and temperatures, each from one of the satellites. Since the data sets are not perfect, and there are gaps in the samples at different places, there is also a population of holes whose wind properties I collected in only one of the satellites.

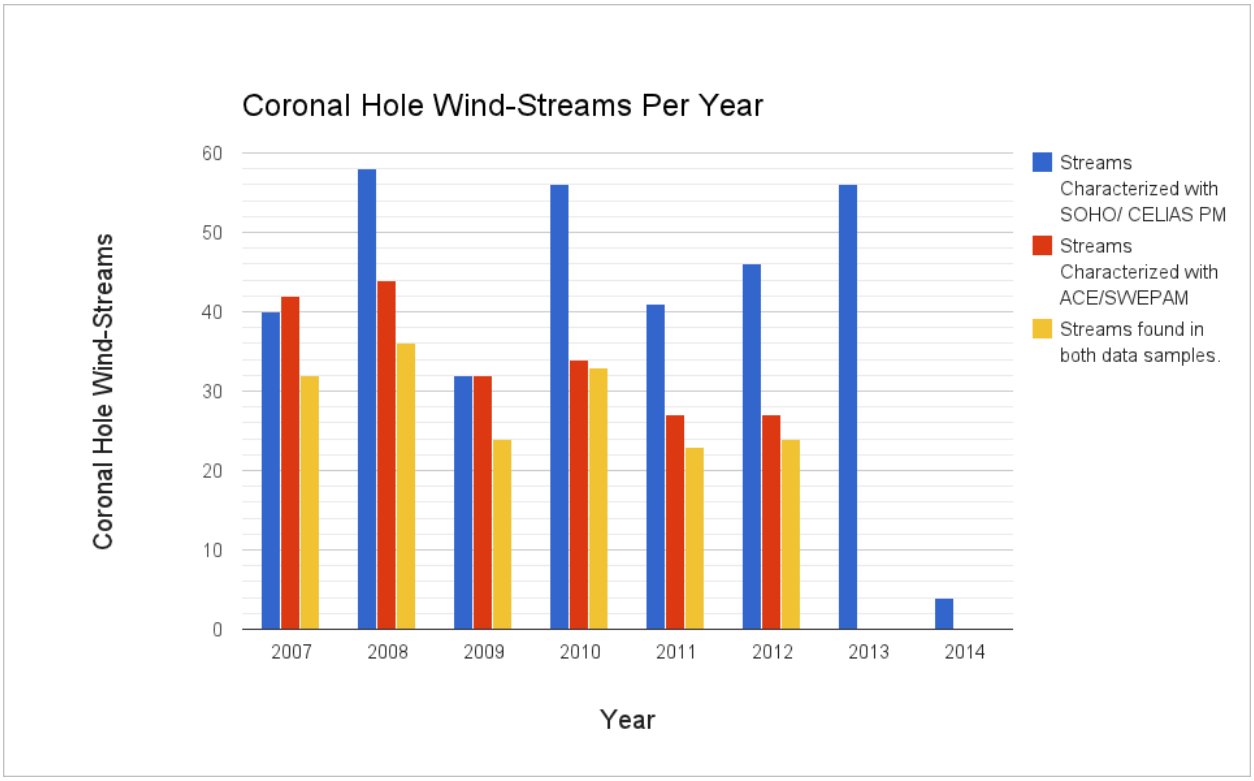

Figure 2.5 Coronal hole wind-streams collected for each year in my survey. Only streams from the month of January are included for the year 2014.

2.3 AREA AND MAGNETIC FIELD DATA COLLECTION

The third part of the project consisted of calculating coronal hole areas and their average magnetic field. To calculate coronal holes areas, I used SOHO/EIT 195 *Å* (January 2007 to June 2010) and SDO/AIA 193 *Å* (June 2010 to February 2014) images of the solar atmosphere. To calculate the average magnetic field strength of each hole, I used line-of-sight (LOS) magnetograms of the solar atmosphere constructed by the *Michelson Doppler Imager* (MDI) aboard SOHO, and the *Helioseismic and Magnetic Field Imager* (HMI), aboard SDO. A magnetogram is a map representation of the observed solar magnetic field strength in the photosphere. (see figure 2.10).

For the calculation of coronal hole areas I used images of each hole as it was roughly centered on the solar disk, such as to have the most direct view possible of the hole (see figure 2.8). The program I created to calculate coronal hole areas was semi-automatic, in the sense that it required user input to select a coronal hole. After clicking on a coronal hole in one of the prepared images, my algorithm would select a 10x10 pixels box around the image pixel that was clicked-on and cross-check the range of intensity values of these pixels with a previously assigned intensity threshold. This intensity threshold was an experimentally derived range of values for the intensity at which coronal holes normally appear in the EUV images used to identify them. If the range of intensities sampled by the 10x10 box fell within the limits of the aforementioned intensity threshold, indicating that the area selected by the human operator met the previously defined constraints for a coronal hole, the program would proceed to check every neighboring pixel that fell within the intensity range of the 10x10 box. If the intensity of these pixels fell

within the established threshold, they too would be counted as belonging to the coronal hole. In this way, the area for the selected coronal hole would expand from the initial 10X10 pixel box until it met the hole's boundary, where the pixel intensity would suddenly become much higher than that of the dark coronal hole pixels.

The mapping from pixel area to physical meter squared (m^2) area was done by first calculating the corresponding area in m^2 for the pixel at the center of the Sun, then scaling this value as a function of latitude to assign area values to every pixel, and finally by summing the area values of those pixels which were selected as being part of the hole. The scaling was necessary since, as figure 2.6 shows, pixels away from the center of the Sun correspond to regions of larger area than those closer to the center.

To calculate the area of the central pixel, I used the small angle approximation of the angular distance formula:

$$d = D\phi, \qquad \text{(eq. 1)}$$

where *d* is the physical length of the sides of the square that the central pixel projects on the solar sphere, *D* is the distance from the imaging spacecraft to the solar corona, and ϕ is the arcsecond per pixel resolution of the coronal hole image. The area of the central pixel is therefore simply d^2. The area of every other pixel A_i, is given by:

$$A_i = d^2/\cos(\theta_i), \qquad \text{(eq. 2)}$$

where θ_i is the centered latitude of the region projected by a pixel *i* on the solar atmosphere.

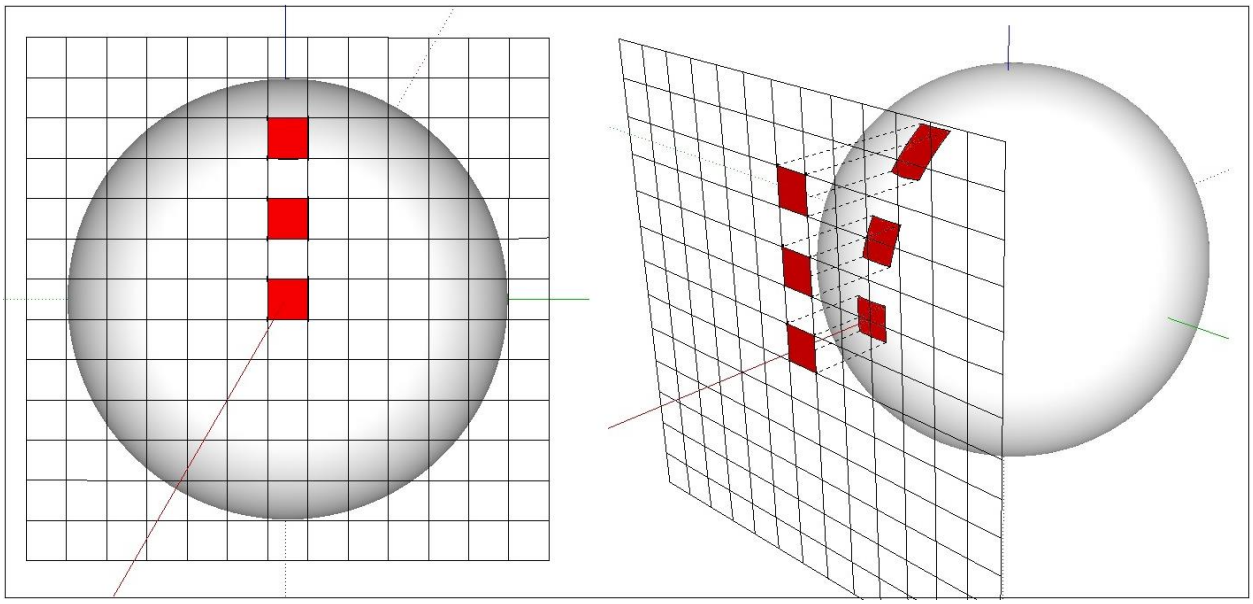

Figure 2.6 Pixel area projection on the solar surface. This image displays the need for scaling required when calculating coronal hole areas. The areas on the solar surface to which each pixel corresponds varies as a function of latitude due to the curvature of the Sun. Pixels away from the pixel corresponding to the center of the Sun correspond to larger areas than those closer to the center.

Technically, the central pixel does not project a true square on the solar atmosphere, but rather a spherical cube, made of curved sides of length *d*. Since *d* is so small compared to the curvature of the Sun, however, approximating *d* to be a line, and thus approximating the projected area into a square, does not significantly affect the accuracy of the measurements.

To calculate the average LOS magnetic strength of a hole, my program would upload a magnetogram of the solar atmosphere taken at the same time as the EUV image used to calculate the hole's area, resize it so that the solar disk in both images mapped pixel to pixel, and select the pixels in the magnetogram which corresponded to coronal hole pixels in the EUV image.

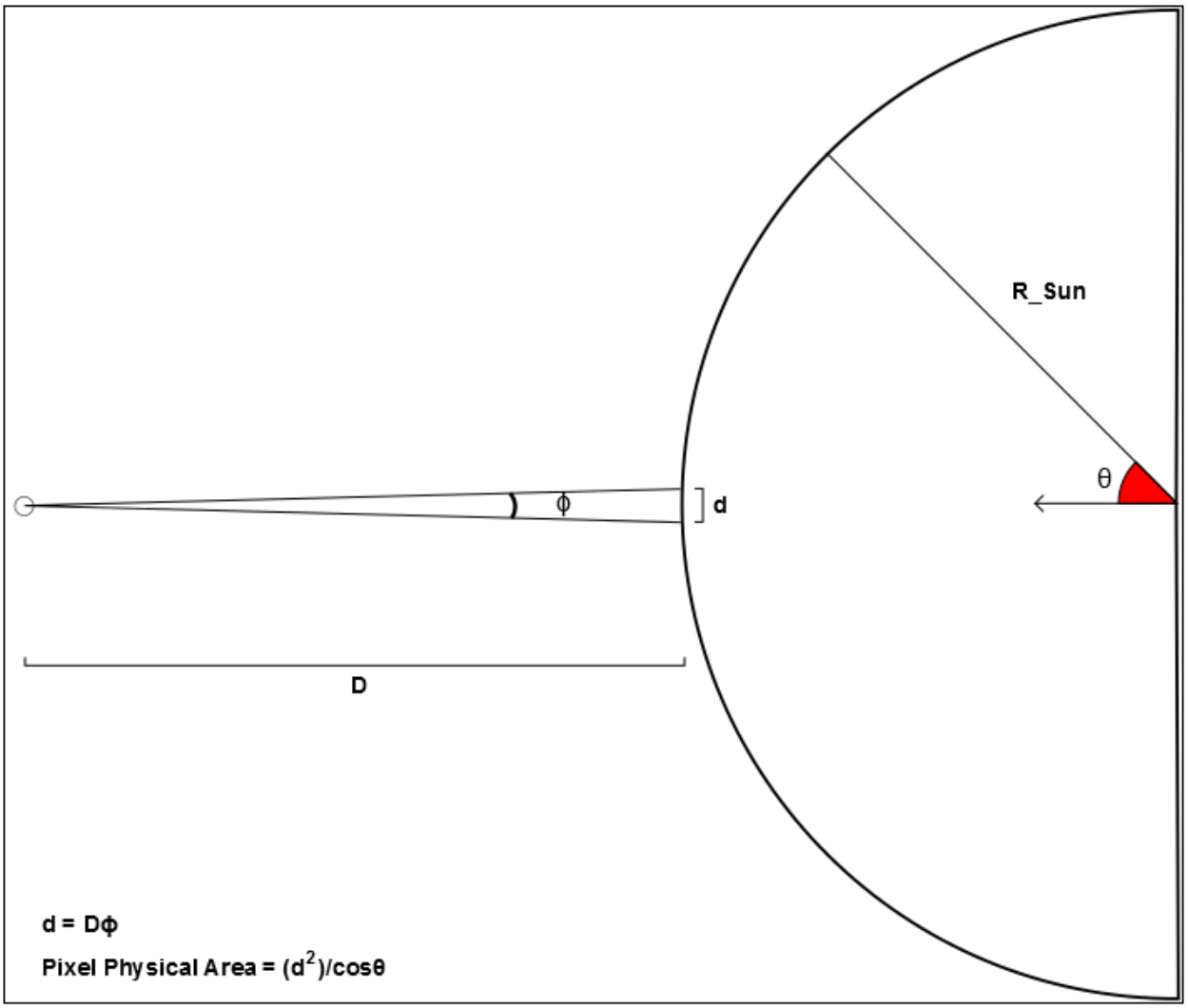

Figure 2.7 Calculating central pixel area, and pixel scaling. In this diagram, ϕ is the arcsecond per pixel resolution of the imaging instrument used to take the pictures with which I calculated coronal hole areas. D is the distance of the instrument to the region covered by the pixel corresponding to the center of the Sun in these images, and d, the physical distance which this pixel projects. Since pixels corresponding to higher latitudes are further away, d, and thus the surface area they project on the solar sphere, is larger, and must be scaled.

In the magnetograms that I used, each pixel contains the LOS magnetic strength value of the area on the solar atmosphere to which the pixel corresponds. Since pixels near the solar limb correspond to larger areas than those near the center of the solar disk, I used a weighted average of the magnetic field strength of each pixel based on each pixel's unique area scaling. The average line of sight magnetic strength of the hole, B_{los}, was thus given by:

$$B_{los} = \Sigma \frac{B_i A_i}{A_t} \quad \text{(eq. 3)}$$

Where B_i was the magnetic field strength value recorded in the magnetogram for a particular pixel *i*, A_i was the latitude-scaled area component calculated for that same pixel, and A_t was the total area of the hole. Figure 2.10 shows the magnetogram I used to calculate the average magnetic field strength of the hole shown in figure 2.8. The area shaded in red corresponds to the area on the solar corona which is covered by this particular hole.

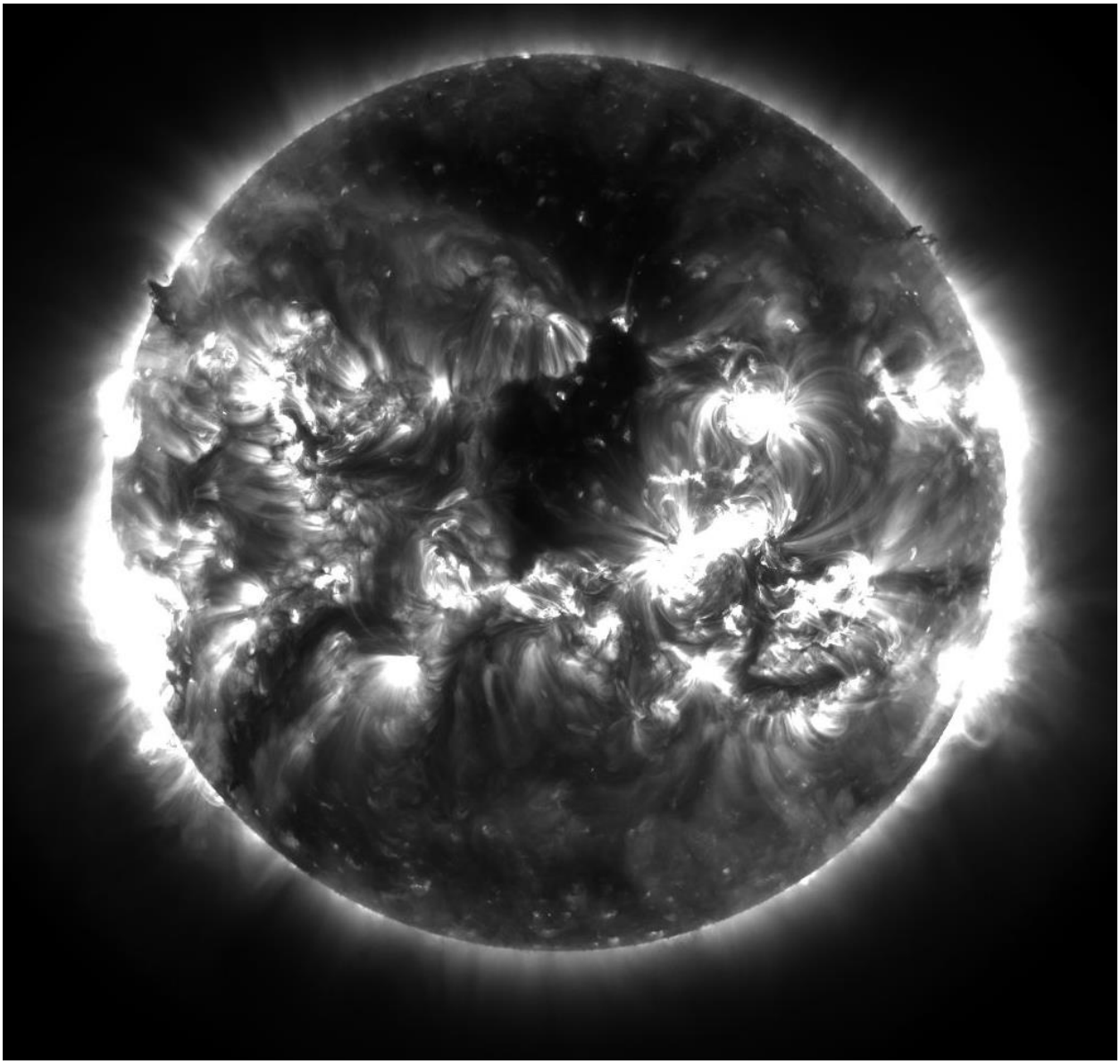

Figure 2.8 195 *Å* image taken by SDO/AIA. A large coronal hole dominates the center of the Sun. This image was used to calculate the area of this particular hole.

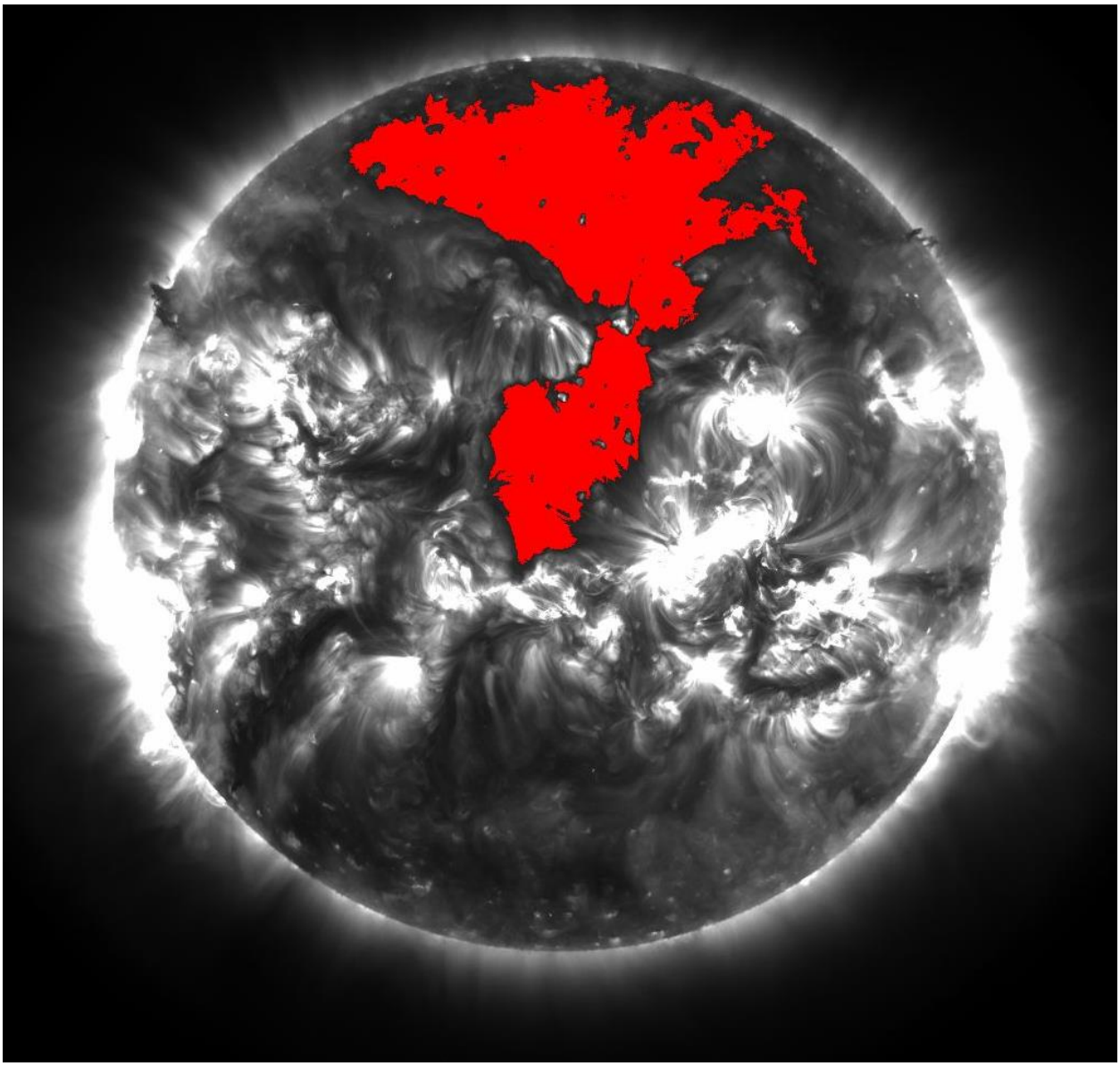

Figure 2.9 The results of the area calculating algorithm for the hole shown in figure 2.8. In this image, every pixel selected by the area calculating code as belonging to the coronal hole has been colored in red by the program to provide visual feedback to the user.

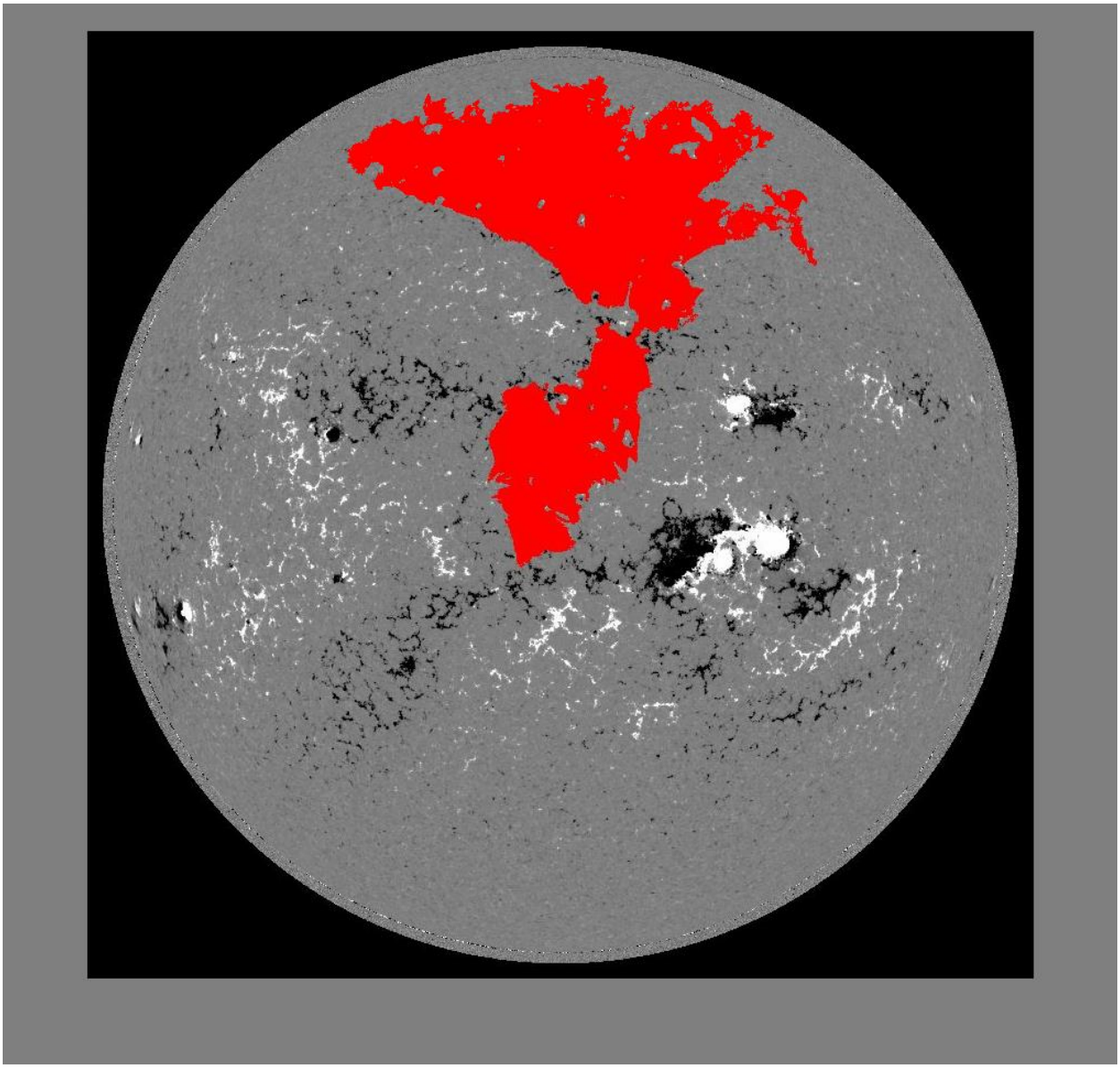

Figure 2.10 SDO/HMI 6173 *Å* magnetogram of the solar photosphere. The pixels in red give visual feedback of the area selected in this map as being part of the large coronal hole identified in figure 2.8. HMI magnetograms assign measurements of LOS magnetic field strength to every pixel. My algorithm selects those pixels within the area of the coronal holes selected and yields a weighted average of their magnetic field strength.

3 RESULTS

3.1 SOLAR WIND-STREAM PROPERTIES

The properties of coronal hole wind streams varied considerably over the seven years surveyed. As seen in figures 3.1 and 3.2, the coronal holes of the years 2007 and 2008 exhibited high wind velocities of approximately 600 km/s. There was a significant drop in wind velocity for the year 2009, where the average coronal hole wind speed was approximately 475 km/s. Wind stream speed reached 2007-2008 levels during the years 2010 and 2011, but dropped again to 2009 levels in 2012, where with the exception of a few large holes, the average wind speed was 460 km/s. The year 2013 exhibited slightly higher velocities than the year 2012, but remained below 2007-2008 levels. The wind streams for the month of January 2014 were of high velocity, at around ~600 km/s. These trends were apparent in both the ACE/SWEPAM and SOHO/CELIAS MTOF PM data samples. The spread in the wind speed values reported by these two instruments for the same wind streams was within 50 km/s for nearly every stream (see figure 3.3).

A comparison between the wind velocity, density, and temperature for the 363 streams that I characterized established that there is an anti-correlation between wind stream velocity and wind stream density (see figures 3.4 and 3.5), and that there is a correlation between wind stream velocity and temperature (see figures 3.6 and 3.7). For those streams that I characterized with ACE/SWEPAM, which provided alpha to proton number density ratios (, I found that there also is a correlation between the ratio of alpha

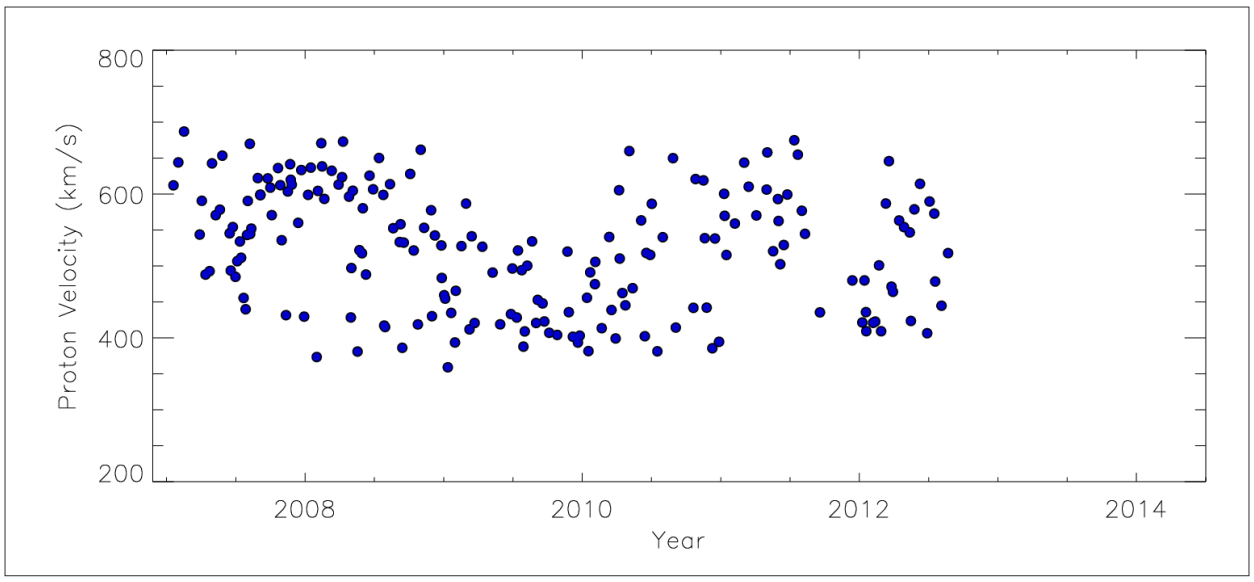

Figure 3.1 Evolution of coronal hole wind-stream velocity at 1 AU from January 2007, through the year 2012, using data recorded by ACE/SWEPAM. The decrease in overall wind speed seen throughout the year 2009 coincides with the rising phase of cycle 24 following the 23-24 minimum (2007-2009). Each circle represents the average wind speed of a coronal hole from the sample. The gaps in the last halves of the years 2011 and 2012 are due to the absence of data for those periods.

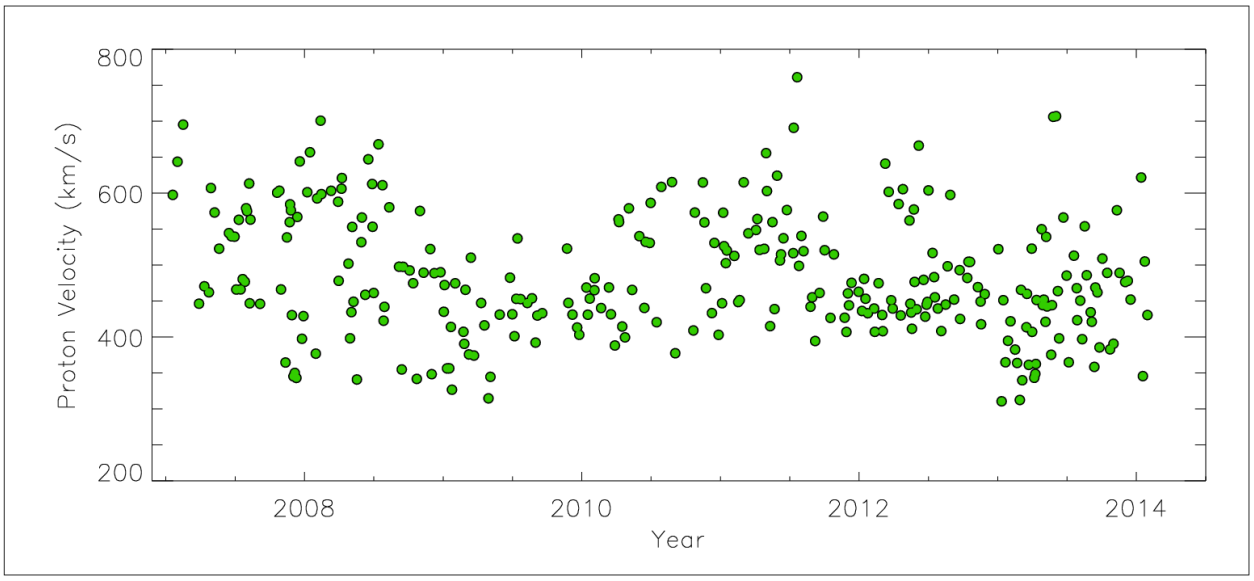

Figure 3.2 Evolution of coronal hole wind-stream at 1 AU velocity from 2007 to 2014 using data recorded by SOHO/CELIAS MTOF Proton Monitor.

particle to proton number density and wind velocity (see figure 3.8). This ratio varied over the solar cycle, but it varied differently for wind streams of different speeds (see figure 3.9 and discussion section).The wind stream mass flux (wind velocity times density) experienced little variation over the years surveyed. The stability of the wind mass flux over the solar cycle, which is the product of the wind velocity and density, is to be expected given the inverse relation between wind stream velocity and density. Nonetheless, there were slight dips in the mass flux throughout the year 2009 and the last half of 2011 and the first half of 2012 (see figures 3.10 and 3.11). The average mass flux for these two periods of time was approximately 20% lower than the average mass flux of the whole survey.

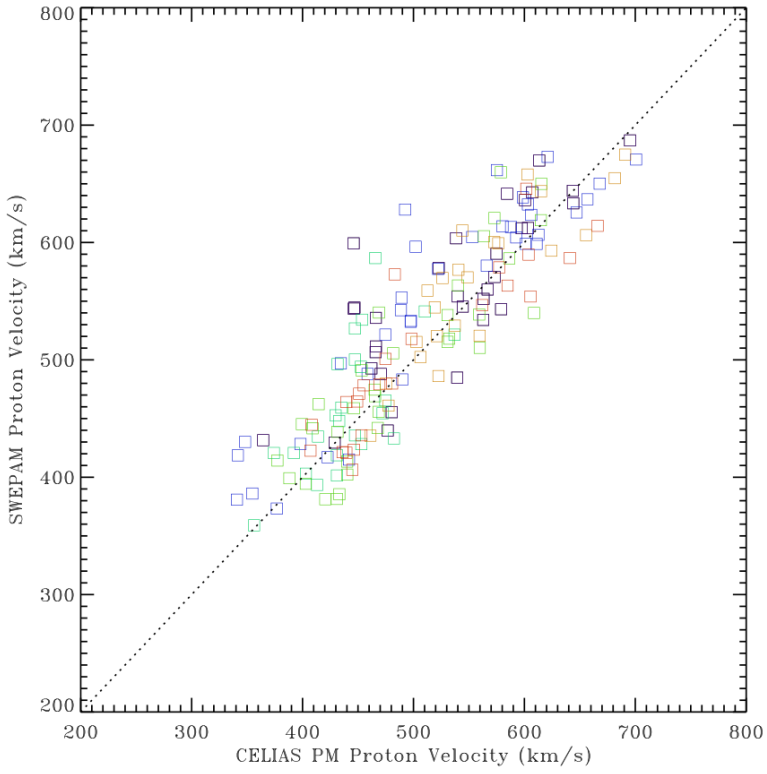

Figure 3.3 Wind velocity measured by ACE/SWEPAM vs. wind velocity measured by SOHO/CELIAS MTOF PM for those streams characterized by both instruments. Different colors indicate different years. On average, the ACE/SWEPAM instrument recorded slightly higher wind velocities than SOHO/CELIAS PM.

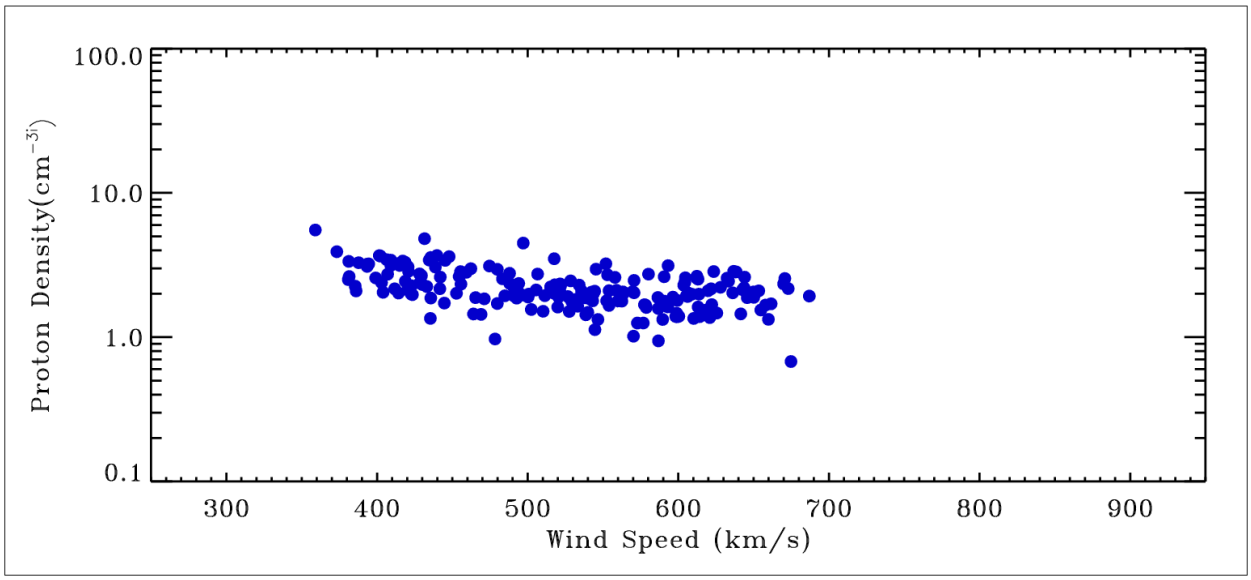

Figure 3.4 Proton density vs. wind Speed at 1 AU, recorded by ACE/SWEPAM from 2007 through the year 2012.

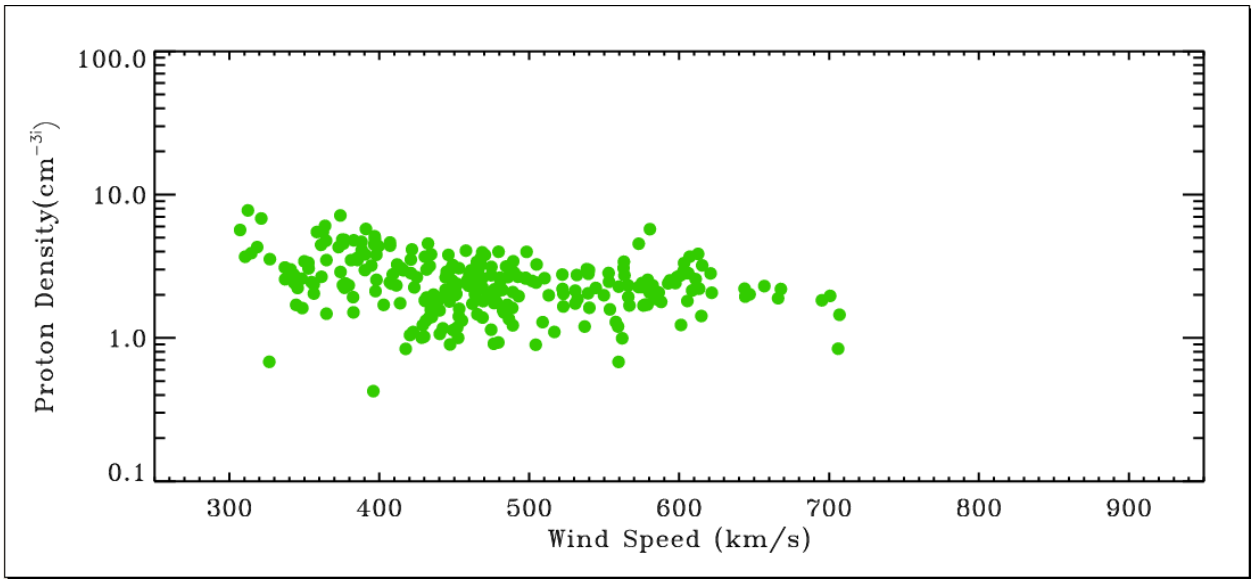

Figure 3.5 Proton Density vs. Wind Speed at 1 AU, recorded by SOHO/CELIAS MTOF Proton Monitor from January 2007 to February 2014.

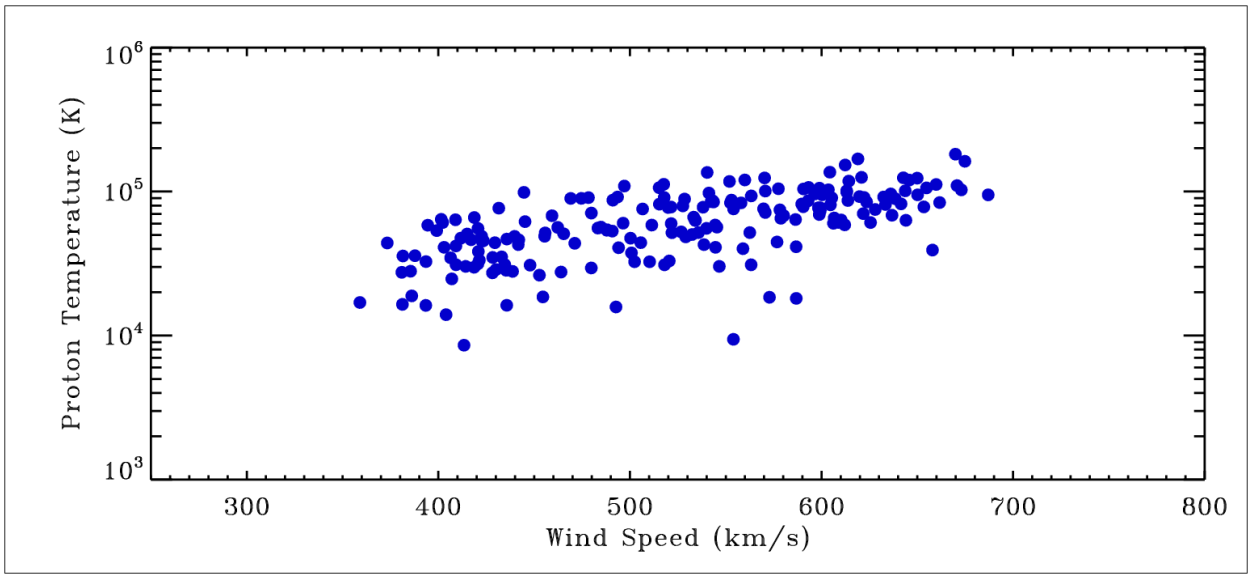

Figure 3.6 Proton Temperature vs. Wind Speed, recorded by ACE/SWEPAM at 1 AU from 2007 through the year 2012.

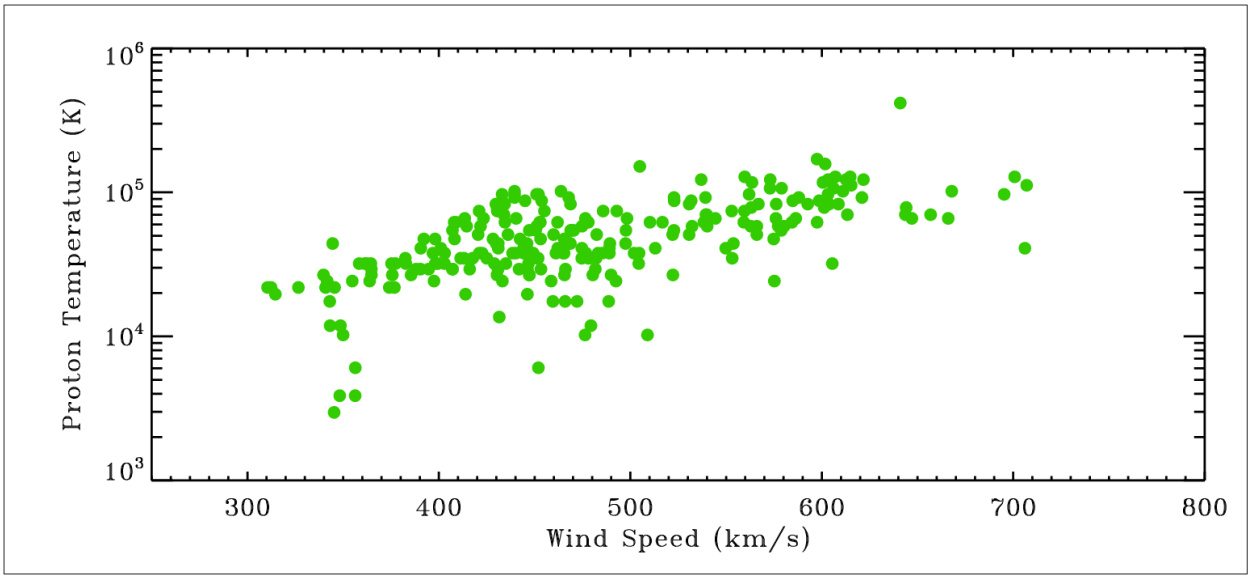

Figure 3.7 Proton Temperature vs. Wind Speed, recorded by SOHO/CELIAS MTOF Proton Monitor at 1 AU from January 2007 to February 2014.

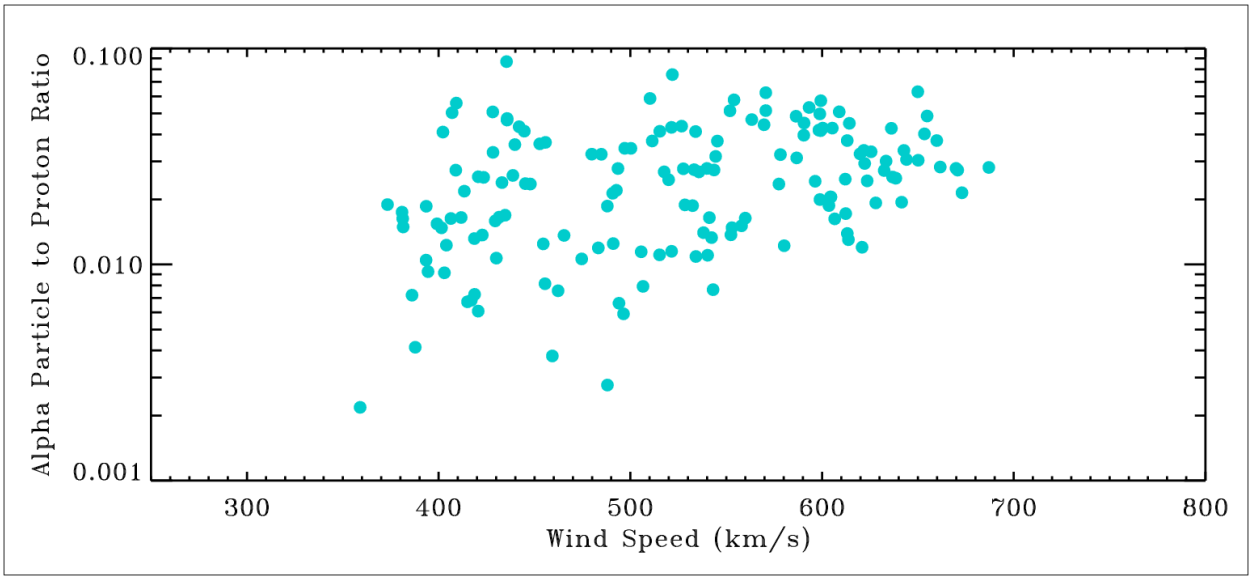

Figure 3.8 The ratio of alpha particle to proton number density vs. wind stream velocity, for ACE/SWEPAM at 1 AU.

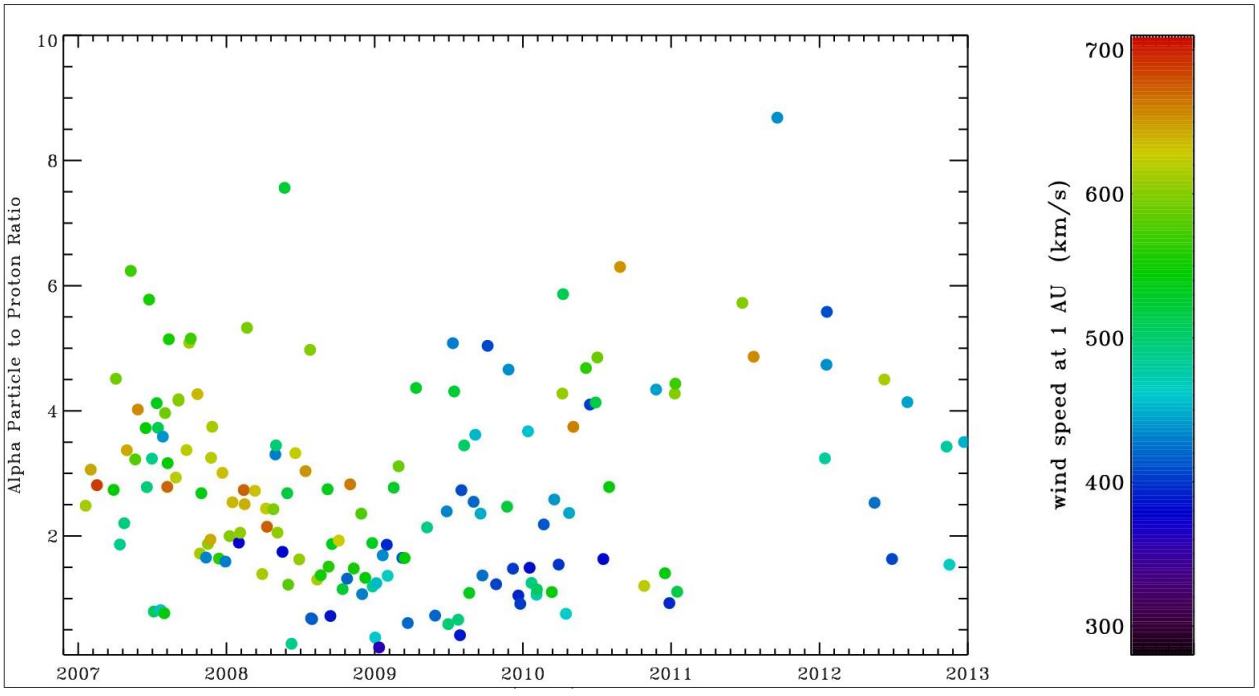

Figure 3.9 Variation of wind stream alpha to proton ratios from 2007 to the end of 2012. Each circle represents the alpha to proton number density ratio of a unique wind stream, colors wind stream velocity. There are far fewer data points for the later years of the survey due to the deterioration of the data recorded by the ACE/SWEPAM instrument. Whereas I was able to collect He+/H+ for every single wind stream from the years 2007 and 2008, I was only able to collect He+/H+ values for 18 out of the 47 wind streams I characterized for the years 2011 and 2012.

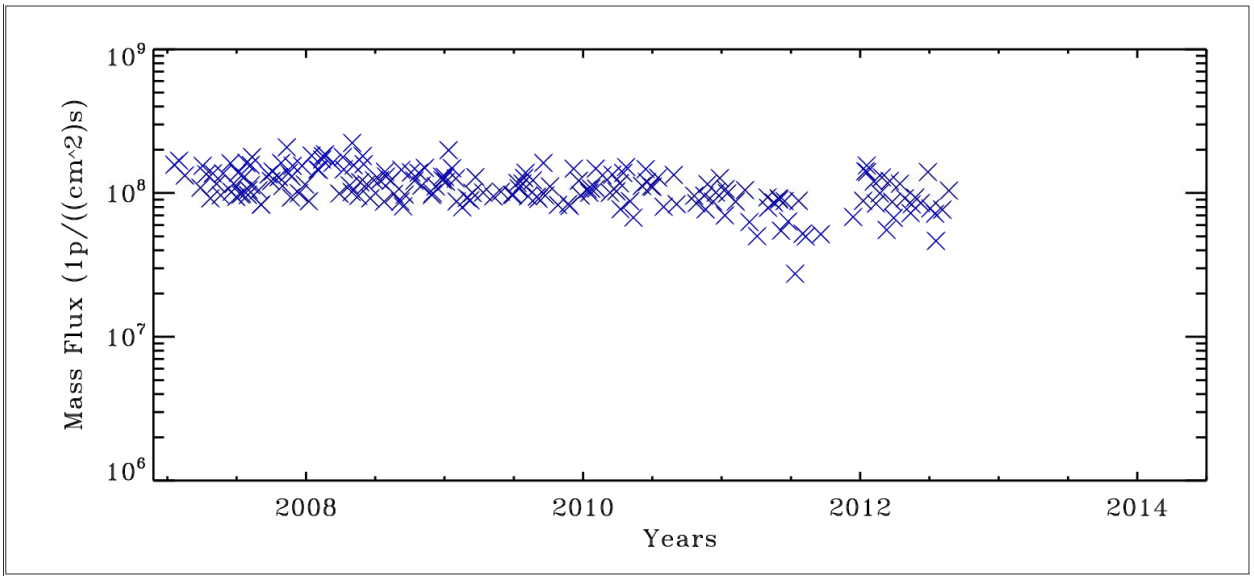

Figure 3.10 Evolution of coronal hole wind stream mass flux from January 2007 through the year 2012 at 1 AU, for ACE/SWEPAM data. There are data real gaps for the last halves of the years 2011 and 2012.

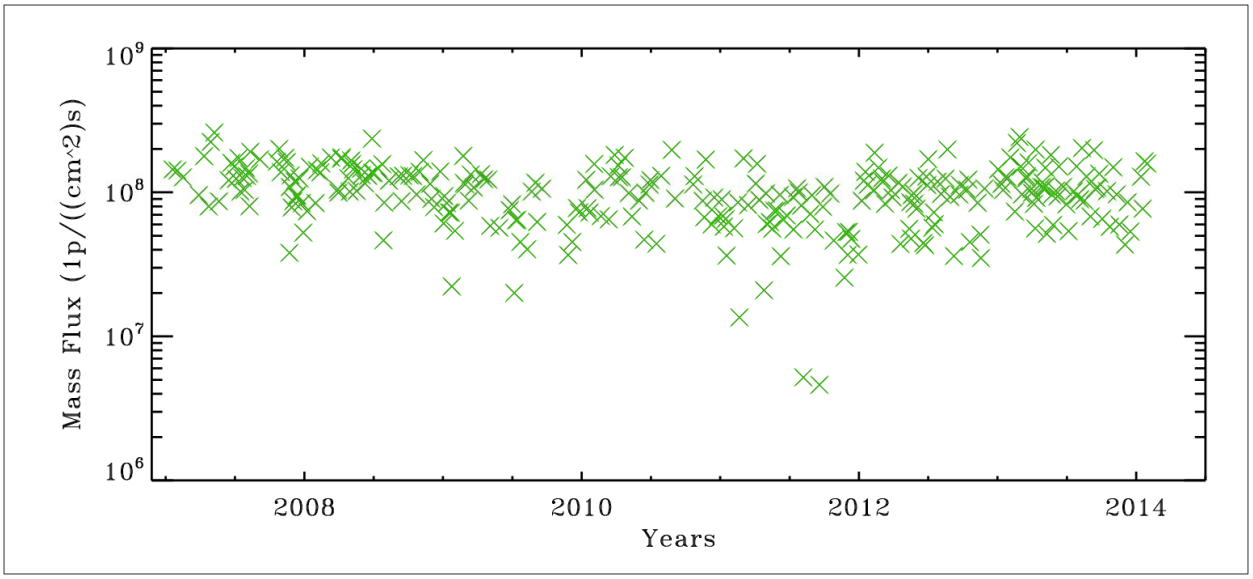

Figure 3.11 Evolution of coronal hole wind stream mass flux from January 2007 to February 2014, for SOHO/CELIAS MTOF PM data.

3.2 AREA AND MAGNETIC FIELD STRENGTH

The comparison of absolute value of the LOS magnetic field strength and coronal hole area as described in section 2.3, shows a negative correlation between coronal hole area and magnetic field strength (see figure 3.12). Comparing magnetic field strength to wind speed also shows a negative correlation between these two properties (see figure 3.13). There is a positive correlation between coronal hole area and wind speed (see figure 3.14). This correlation is steeply linear up to coronal hole areas of 1017 m2, but flattens out henceforth, indicating that after reaching this size, gains in area do not translate into higher velocities. This also suggests a peak velocity of ~700 km/s for the wind streams of the last seven years. In summary, our results indicate that smaller holes have larger magnetic field strength values, and slower winds.

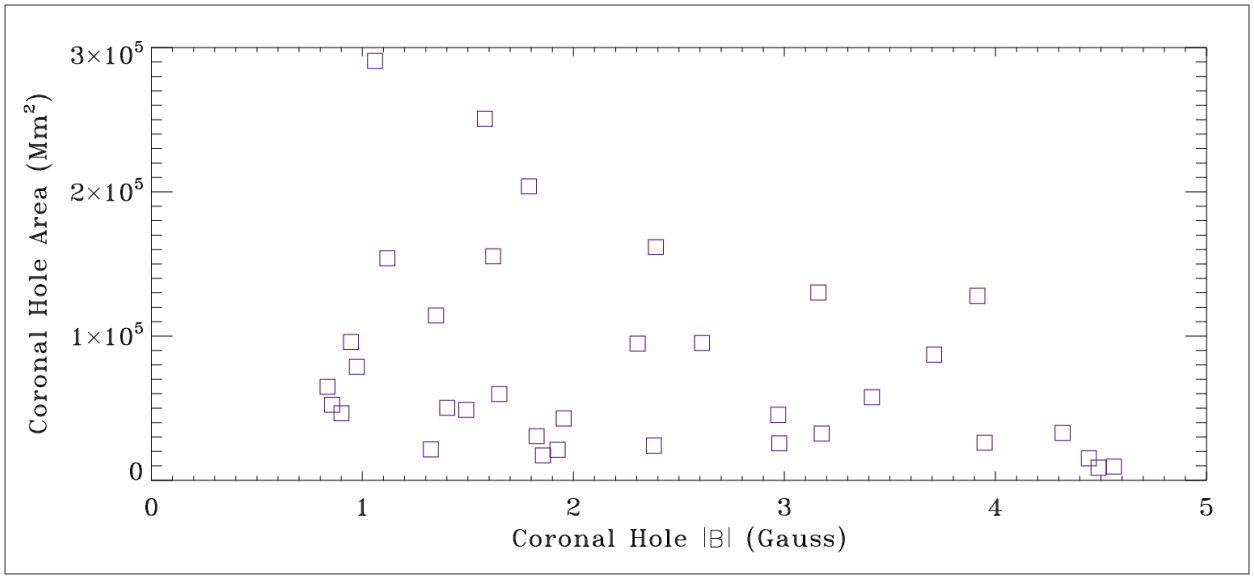

Figure 3.12 Coronal hole area vs. absolute coronal magnetic field strength.

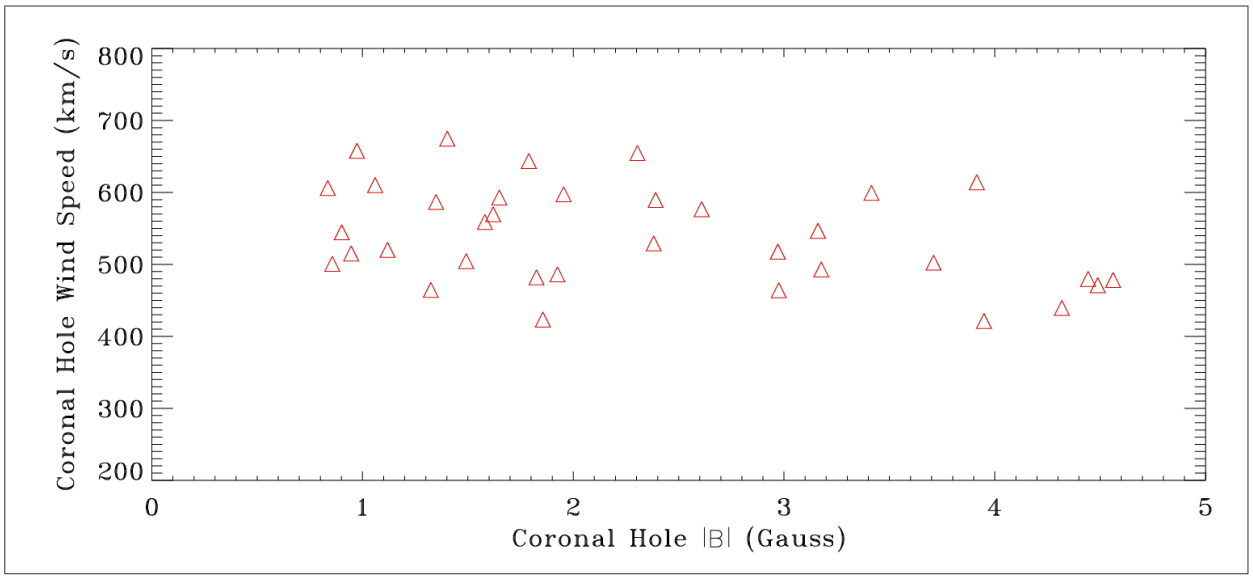

Figure 3.13 Coronal hole wind speed vs. absolute coronal magnetic field strength.

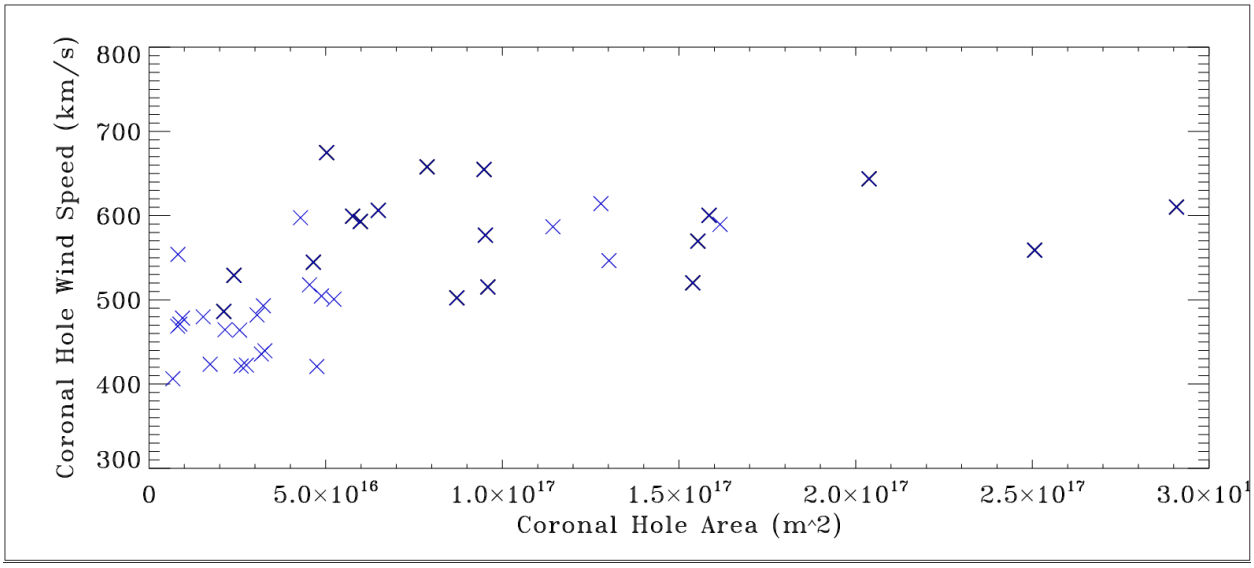

Figure 3.14 Coronal hole wind speed vs. coronal area.

4 DISCUSSION AND FUTURE WORK

Some of the relationships that I determined for the coronal holes of the first seven years of solar cycle 24, were also established by Miralles et al (2006, 2007) for the coronal holes of solar cycle 23. However, Miralles *et al.* encountered more extreme plasma properties for the previous cycle than I have for the current cycle. The speed of the wind streams from solar cycle 23 studied by Miralles *et al.* (2006, Figure 1) were between 450 and 775 km/s for a sample of ~200 large equatorial coronal holes. The velocity of the wind streams for my study of solar cycle 24 equatorial coronal holes range from 350 to 700 km/s. The study by Miralles *et al.* targeted larger holes because of their requirement to obtain UV spectroscopic readings of the holes at the solar limb, this may explain why their lower velocity limit was not as low as mine. The differences in wind ceilings from our two studies, however, does not seem to arise from any bias, but rather from an actual lower velocity peak exhibited by the coronal hole wind streams of the current cycle. It is interesting that the population of large low-latitude holes seen for the first time in the solar minimum between solar cycle 23 and the current cycle, despite exhibiting comparable areas, do not reach as high wind speeds.

The alpha to proton ratio density of the coronal hole wind streams shows a strong dependence on the levels of solar activity in the cycle. The average ratios are overall smaller during solar minimum and larger during solar maximum, but differ for wind streams of different speeds (see figure 3.9). The average ratios for high-speed wind range from 4 (solar minimum 2007-2009) to 6 (solar maximum 2011 to 2014), whereas for the slow-speed wind streams they vary from 1.5 (solar minimum) to 3.5 (solar maximum).

The correlation between wind stream speed and the relative abundance of helium to hydrogen ion number density shown by the coronal holes of the current cycle is similar to that established by Kasper et al (2007) for the coronal hole wind streams of solar cycle 23. What the physical process is that causes this correlation is still not understood.

Cycle 24 has shown the lowest levels of photospheric solar activity for the last 50 years. Although the cycle exhibited a population of large low latitude coronal holes during solar minimum, contributing to the fast component of the solar wind at a time when normally only polar coronal holes are seen, the properties of these holes were similar to those of the large low latitude holes seen during solar maximum. Overall, the highest solar wind proton speeds achieved by the fastest wind streams of the current cycle were ~75 km/s lower than those of the previous cycle, and the relation to current weaker solar activity is not yet understood.

This project is the largest survey of coronal hole properties for cycle 24. Although I've been able to establish some important trends for the behavior of the plasma properties of the coronal holes and their associated wind streams for this cycle, and their relation to coronal hole area and magnetic field strength, a proper comparison to the same properties for the coronal holes of cycle 23 has not yet been carried out. Future work will involve an in-depth comparison of the trend variations between the two cycles, and an exploration of the physical processes most likely to be the drivers of these trends, along with continuous monitoring of the properties of the current cycle, predicted to end around 2020. Future work will also involve the employment of the various plasma properties I've collected as constraints for solar wind theoretical models, in particular, those seeking to explain coronal heating.

5 ACKNOWLEDGEMENTS

I would like to extend my thanks to Professor Jim Moran, whose stern, yet kind guidance over the last two semester ensured not only that this work was completed in time, but that it was accessible to readers who are not experts in solar physics. Jim's sharp sense of humor, and biting, yet insightful comments made our regular Monday meetings an enjoyable and fruitful time.

I would also like to thank Dr. Steven Cranmer, for taking the time to proof read my final work, and for indirectly having taught me the basics of coronal hole physics. Throughout this process, Dr. Cranmer was a semi-mythological figure whose name I would mention in whispers in Dr. Miralles office, and whose past writings I poured over in order to acquire the necessary background knowledge to carry out my research. His 2009 Coronal Holes review was an excellent starting point for someone who like me, was a novice to the study of this fascinating subject.

Lastly, and most importantly, I would like to thank Dr. Mari Paz Miralles for everything she has done these past two semesters to ensure both the success of this project, and my of own personal growth as a student and as a scientist. No other mentor or teacher in my four years at Harvard College has demonstrated as much commitment, passion for teaching, and accessibility as Dr. Miralles. I feel that aside from being my mentor and teacher, Dr. Miralles has become a friend. I would trust her to be my emergency contact. Without her, this project would never exist, and my senior year would have been a much less didactic, thrilling, and worthwhile experience. Thank you Dr. Miralles, you are the best teacher I've ever had.

6 REFERENCES

Altschuler, M.D., Trotter, D.E., Orrall, F.Q., 1972, “Coronal Holes”, *Solar Phys.*, **26**, 354–365.

Cranmer, Steven R., 2009, “Coronal Holes”, *Living Rev. Solar Phys.*, **6**, 3., URL(accessed <12/21/2013>): http://www.livingreviews.org/lrsp-2009-3

Fisher, R., Sime, D.G., 1984, “Solar activity cycle variation of the K corona”, *Astrophys. J.*,**285**, 354–358.

Huber, M.C.E., Foukal, P.V., Noyes, R.W., Reeves, E.M., Schmahl, E.J., Timothy, J.G., Vernazza, J.E., Withbroe, G. L., 1974, “Extreme-ultraviolet observations of coronal holes: Initial results from Skylab”, *Astrophys. J. Lett.*, **194**, L115–L118.

Hundhausen, A.J., 1972, *Coronal Expansion and the Solar Wind*, vol. 5 of Physics and Chemistry in Space, Springer, Berlin; New York

Krieger, A.S., Timothy, A.F., Roelof, E.C., 1973, “A Coronal Hole and Its Identification as the Source of a High Velocity Solar Wind Stream”, *Solar Phys.*, **29**, 505–525.

Kasper, Justin C., *et al.* 2007 ApJ **660** 901, “Solar Wind Helium Abundance as a Function of Speed and Heliographic Latitude: Variation Through a Solar Cycle.

McComas, D. J., Elbert, R. W., Elliot, H. A., *et al* 2008, Geophys. Res. Lett., 35, L18103 (2008)

Miralles, M. P., Cranmer, S. R., Kohl, J. L. 2001a, “Comparison of Empirical Models for Polar and Equatorial Coronal Holes”, The Astrophysical Journal, Volume **549**, Issue 2, pp. L257-L260

Miralles, M. P., Cranmer, S. R., Kohl, J. L. 2001b, ”Ultraviolet Coronagraph Spectrometer Observations of a High-Latitude Coronal Hole with High Oxygen Temperatures and the Next Solar Cycle Polarity”, The Astrophysical Journal, Volume **560**, Issue 2, pp. L193-L196

Miralles, M. P., Cranmer, S. R., Kohl, J. L. 2002, “Cyclical variations in the plasma properties of coronal holes”, In: Proceedings of the SOHO 11 Symposium on From Solar Min to Max: Half a Solar Cycle with SOHO, 11-15 March 2002, Davos, Switzerland. A symposium dedicated to Roger M. Bonnet. Edited by A. Wilson, ESA SP-508, Noordwijk: ESA Publications Division, ISBN 92-9092-818-2, 2002, p. 351 - 359

Miralles, M. P., Cranmer, S. R., Kohl, J. L. 2004,”Low-latitude coronal holes during solar maximum”, Advances in Space Research, Volume **33**, Issue 5, p. 696-700

Miralles, M. P., Cranmer, S. R., Kohl, J. L. 2006, “*Coronal Hole Properties During the First Decade of UVCS/SOHO”*, SOHO-17: 10 Years of SOHO and Beyond, Proceedings of the conference held 7-12 May, 2006 at Giardini Naxos, Sicily, Italy. Edited by H. Lacoste and L. Ouwehand. ESA SP-617. European Space Agency, 2006. Published on CDROM, p.15.1

Miralles, M. P., Cranmer, S. R., Kohl, J. L. 2007, “Towards the UVCS Coronal Hole Atlas for Solar Cycle 23: The Data”, American Astronomical Society Meeting 210, #30.05; Bulletin of the American Astronomical Society, Vol. **39**, p.143

Miralles, M. P., Cranmer, S. R., Panasyuk, A. V., Uzzo, M. 2010, “The Tale of Two Minima and a Solar Cycle in Between: An Ongoing Fast Solar Wind Investigation”,SOHO-23: Understanding a Peculiar Solar Minimum ASP Conference Series Vol. **428**, proceedings of a workshop held 21-25 September 2009 in Northeast Harbor, Maine, USA. Edited by Steven R. Cranmer, J. Todd Hoeksema, and John L. Kohl. San Francisco: Astronomical Society of the Pacific, 2010, p.237

Munro, R.H., Withbroe, G.L., 1972, “Properties of a Coronal ‘hole’ Derived from Extreme-Ultraviolet Observations”, *Astrophys. J.*,**176**, 511–520

Pneuman, G.W., 1973, “The Solar Wind and the Temperature-Density Structure of the Solar Corona”, *Solar Phys.*, **28**, 247–262.

Noci, G., 1973, “Energy Budget in Coronal Holes”, *Solar Phys.*, **28**, 403–407.

Saito, K., 1958, “Polar Rays of the Solar Corona”, Publ. Astron. Soc. Japan, 10, 49–78.

Wilcox, J.M., 1968, “The Interplanetary Magnetic Field. Solar Origin and Terrestrial Effects”, *Space Sci. Rev.*, **8**, 258–328.